Title

The focus thermal study around the spreading center of southwestern Okinawa trough

Authors

Chen, Liwen
Chiang, Hsieh-Tang
Wu, Jyun-Nai
et al.

Publication Date

2020-12-01

DOI

10.1016/j.tecto.2020.228649

Tectonophysics 796 (2020) 228649

Contents lists available at ScienceDirect

Tectonophysics

journal homepage: www.elsevier.com/locate/tecto

The focus thermal study around the spreading center of southwestern Okinawa trough

Liwen Chen [a,b], Hsieh-Tang Chiang [c,*], Jyun-Nai Wu [d], Ling-Yun Chiao [e], Chuen-Tien Shyu [e], Char-Shine Liu [b], Yunshuen Wang [f], Song-Chuen Chen [f]

[a] Marine Science and Information Research Center, National Academy of Marine Research, Ocean Affair Council, Taiwan
[b] Ocean Center, National Taiwan University, Taiwan
[c] Center for General Education, National Ilan University, Taiwan
[d] Scirpps Institution of Oceanography, University of California San Diego, United States of America
[e] Institute of Oceanography, National Taiwan University, Taiwan
[f] Central Geological Survey, MOEA, Taiwan

ARTICLE INFO

Keywords:
Hydrothermal vents
Geolin mound
Heat flow
South Okinawa trough

ABSTRACT

Voluminous hydrothermal systems are corresponding to the heat flow anomaly discovered from previous geophysical surveys in the Southern Okinawa Trough (SOT), which is an area with a high sedimentation rate supplied by the East China Sea shelf and the island of Taiwan. Our latest fifteen field measurements around the Geolin Mound (GLM) (24° 36.6 'N, 122° 53'E) are located at a sedimentary basin west of the Yonaguni Rift, which is nearby the southwestern tip of a NE-SW trending volcano trail in the SOT. The heat flow results illustrate a concentric decrease from 31,477 to 180 mW/m^2 in a 1-km radius around the GLM, evidently proving the focus fluid migration along the major fluid conduit. The ultrahigh temperature observations revealed the existence of magmatic components in shallow sediments. Combining the subsurface profiles with the temperature fields around the GLM, a 0.16-km^2 acoustic blanking area of the G1 fluid conduit was recognized from the chirp sonar image and numerous interpreted igneous reflections with fluids related features from seismic profiles. As a result, we proposed a conceptual model, which simultaneously illustrates the hydrothermal circulation pattern from the previous general surveys and the enormous thermal anomaly from current detailed measurements. The sill-to-sill feeding sedimentary basin of the GLM is capable of demonstrating the enormous thermal anomaly around the spreading center of the SOT and appropriately represents the potential hydrothermal discharge and recharge by heat flow distribution around the GLM.

1. Introduction

The global oceanic heat flux was predicted to be 32×10^{12} W and approximately 34% comes from hydrothermal flow (Stein and Stein, 2012). Hydrothermal circulation is commonly detected from the young ocean and backarc basins, which causes some extreme heat flows that have been observed in small basins (Yamano et al., 1989). Hydrothermal vent areas show complex flow patterns with extremely high heat flows close to low heat flows. Although most vigorous vents are near spreading centers, older crust isolated crystalline crust outcrops surrounded by a well-deposited area can also vent measurable amounts of hydrothermal fluid (e.g., the Flank Flux survey area on the Juan de Fuca plate) (Stein and Von Herzen, 2001). Sightings of active hydrothermal phenomena, such as black smokers, have been reported at sites of the spreading centers of the Pacific Ocean and the Atlantic Ocean, and hydrothermal polymetallic sulfide and chimneys with living biota have been reported from some backarc basins. Detailed heat flow surveys for hydrothermal system studies have become prevalent in recent decades (Kimura et al., 1988).

Submarine hydrothermal activities with volcanic features and formations have been discovered in the Okinawa Trough (OT) and the distribution is controlled principally by tectonic factors (Glasby and Notsu, 2003). Sulfide and sulfate mineralization associated with hydrothermal activity recognized in hydrothermal fields of the OT is commonly represented by the coexisting occurrence of zinc- and lead-enriched polymetallic sulfides and abundant sulfate minerals (Izawa

* Corresponding author.
E-mail address: d92241007@ntu.edu.tw (H.-T. Chiang).

https://doi.org/10.1016/j.tecto.2020.228649
Received 23 September 2019; Received in revised form 5 October 2020; Accepted 8 October 2020
Available online 18 October 2020

et al., 1991). Besides, the hydrothermal carbonate chimneys mound with high contents of Au, Ag, and As were detected in the basin sediments in the middle Okinawa Trough (MOT) (Izawa, 1991). This uniqueness greatly attracted scientists' interest to work on hydrothermal deposits to uncover their geological significance and mineralogy (Zhang et al., 2018). Previous studies have suggested that hydrothermal activities with enormous heat flows are generally located in the rift belt in the axial part of the OT, which is undergoing the most intense normal faulting with large-scale variation in heat flow (Fig. 1) (Liu et al., 2016; Luo, 2001).

The heat flow studies in the OT backarc region illustrated large bumpy values, which are consistent with the records of backarc regions worldwide (Gutscher et al., 2016) and the cooling effect in sedimentary basins (Turcotte and Ahern, 1977). Heat flows in the OT are high (10^2 to 10^5 mW/m^2) and related to the well-developed continental rifting and initial seafloor spreading because of the crustal disequilibrium, even though the seafloor spreading had caused relatively low heat flow (Kinoshita and Yamano, 1997), the extremely high heat flow can be up to 72,000 mW/m^2 at "Jade" hydrothermal venting site in the MOT (Glasby and Notsu, 2003). The heat flow fluctuation, across the hydrothermal vents of Yonaguni Knoll IV (YK4) in the southern Okinawa Trough (SOT), varies from 10 to 3200 mW/m^2 over a distance of 2 km (Suzuki et al., 2008; Wu et al., 2019). The shallow-level heat source results in hydrothermal circulation or convective cells on large and small scales have been proposed to explain these drastic heat flow fluctuations (Kinoshita and Yamano, 1997). Many volcanic formations and features have been discovered in the OT, including the black smoker vents with high fluid temperature (323 °C) in Tiger and Lion Chimney sites located at YK4 (Inagaki et al., 2006). The venting mechanism is regarded to be driven by magmatic sources and the resulting buoyancy forces from hot water to migrate to the surface as hydrothermal vents often emitted into the sea along weak fractures with metal and sulfide materials (Sakai et al., 1990). Hydrothermal circulation facilitates a major chemical exchange between the circulating seawater and the ocean crust, and plays an important role in regulating the chemistry of the oceans (e.g., Elderfield and Schultz, 1996). Thus, studying the in-situ measured geophysical data to interpret the hydrothermal activity may better understand the regional fluid migration pattern in space, which might affect the potential mineralization in the SOT. In this study, we reported the fifteen latest field measurements within a 3-km^2 area around Geolin Mound (GLM), a hydrothermal mound situated at a sedimentary basin west of YK4 in the SOT (Fig. 1), combined with the subsurface seismic images to access the regional hydrothermal regime.

2. Background studies

The OT is a back-arc spreading center in the rifting stage, generated as a result of the Philippine Sea Plate subducting beneath the Eurasian Plate (Lee et al., 1980; Letouzey and Kimura, 1986; Sibuet et al., 1998), the spreading center extends southwestward to northeastern Taiwan. Tectonically, a southward drift of the South Ryukyu Arc reaches 7 cm/year in Yonaguni (Nakamura, 2000), which makes the convergence in the Ryukyu trench much less oblique and implies a rapid southward trench rollback (Lallemand et al., 2013); topographically, the OT extends from the Ilan Plain in northeastern Taiwan to Kyushu Island in southern Japan (Fig. 1a). Low-velocity zones with high Vp/Vs anomaly suggest the influence of arc magmas beneath the volcanoes at about 10 km and some mantle materials flowing upward from deeper than 50 km

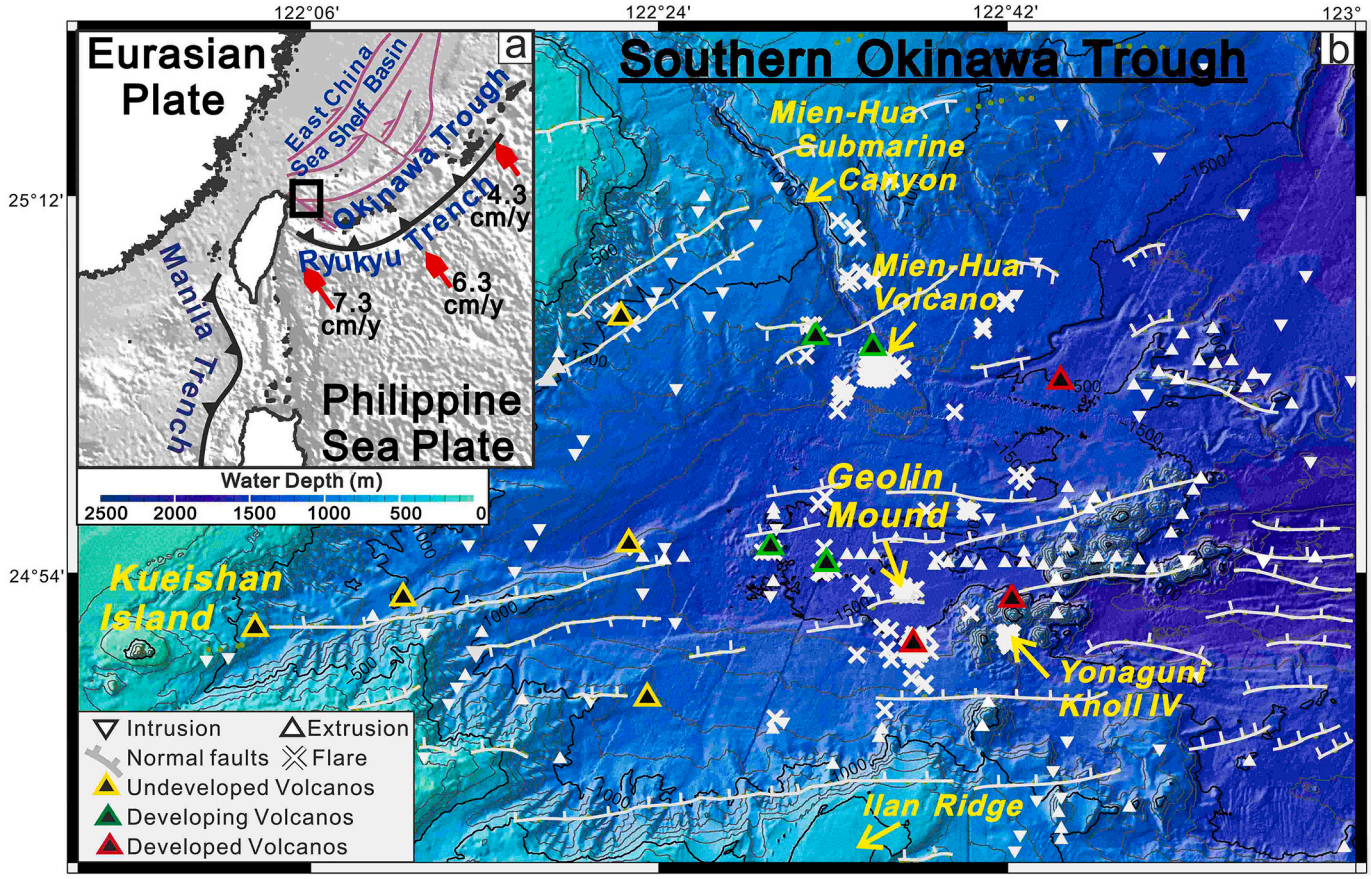

Fig. 1. The geological framework of the SOT (Luo, 2001). (a) The regional tectonic setting around Taiwan while the series normal faults extended the OT backarc basin NE off Taiwan (red arrows) (Gao et al., 2008). (b) The regional feature structure in the SOT defined by previous marine geological survey data. (For interpretation of the references to colour in this figure legend, the reader is referred to the web version of this article.)

along the trough (Nakamura, 2000).

All the three segments of OT (SOT, MOT, and NOT) display the high heat flow and active tectonic deep bathymetry, while they are composed of different structural patterns (Gao et al., 2008) (Fig. 1a). Han et al. (2007) suggested the crustal thickness of the OT increase from 14 to 28 km through analyzing the bathymetry and gravity data. The MOT and SOT, generating the new oceanic crust at the spreading center, are interpreted as the early stage of seafloor spreading by comparing with the global passive continental margins in West Pacific, while the NOT is at the mature stage of continental rifting possessed the character of transitional crust (Liu et al., 2016). Furthermore, the subduction rate of the Philippine Sea Plate (PSP) increased from 4.9 to 7.3 cm/year, from north to south, accelerating the opening of the SOT where the thickest Quaternary sediments were deposited (Li, 1988) (Fig. 1a). Geological evidence suggests the SOT was initially rifted in the mid-to-late Miocene, and the second rifting restarted in Pliocene after cessation of tectonic activity in five ma. (Kimura, 1985; Sibuet et al., 1995), while the geophysical surveys have demonstrated that the SOT is still in the continental rifting stage (Hirata et al., 1991) through the mapping of the normal faults associated with previous earthquakes and volcanic activities in the E-W direction within the extensional grabens (Kao and Rau, 1999) (Fig. 1).

Combining the seismicity with the profile images and Vp models derived from the numerous reflection and refraction seismic data, Nishizawa et al. (2019) presented the crustal thinning structure due to OT backarc rifting to indicate that there are more volcanic intrusions in the south than the north (Fig. 2a). The Vp model of the ECr4 profile along 123°E at Yonaguni Rift (YR) suggests that there is high velocity attenuation at 5–10 km, which is related to the volcanic intrusion (Fig. 2b), while crustal thinning (25 to 15 km) is currently in progress along the entire SOT. Based on the previous geophysical survey, Lu et al. (1981) regarded the low heat flows as probably resulting from hydrothermal circulation in an area of large relief, while Yamano et al. (1989) suggested the high heat flow anomaly may be caused by present or recent hydrothermal activities associated with the rifting process. Liu et al. (2016) suggested the heat flow observations indicate that the SOT spread faster than the MOT. On the other hand, core sample analysis demonstrates that sedimentation rates generally decrease with increasing water depth or distance to offshore, barring a localized depression below the 1400 m isobath where sediment deposition is enhanced by episodic inputs of turbidites (Huh et al., 2006); therefore, the SOT is an area with a high sedimentation rate (10–30 cm/ky) supplied from the East China Sea shelf (Fig. 1a) and the island of Taiwan (Xiong et al., 2018). They possibly dominated the heat flow anomalies in the SOT, besides the voluminous hydrothermal systems (Shyu and Liu, 2001). Furthermore, Chouet (1996) had proposed a seismic model to define the relatively lower frequency earthquakes, characterized by unclear P and S wave arrival, were regard to most of the tectonic

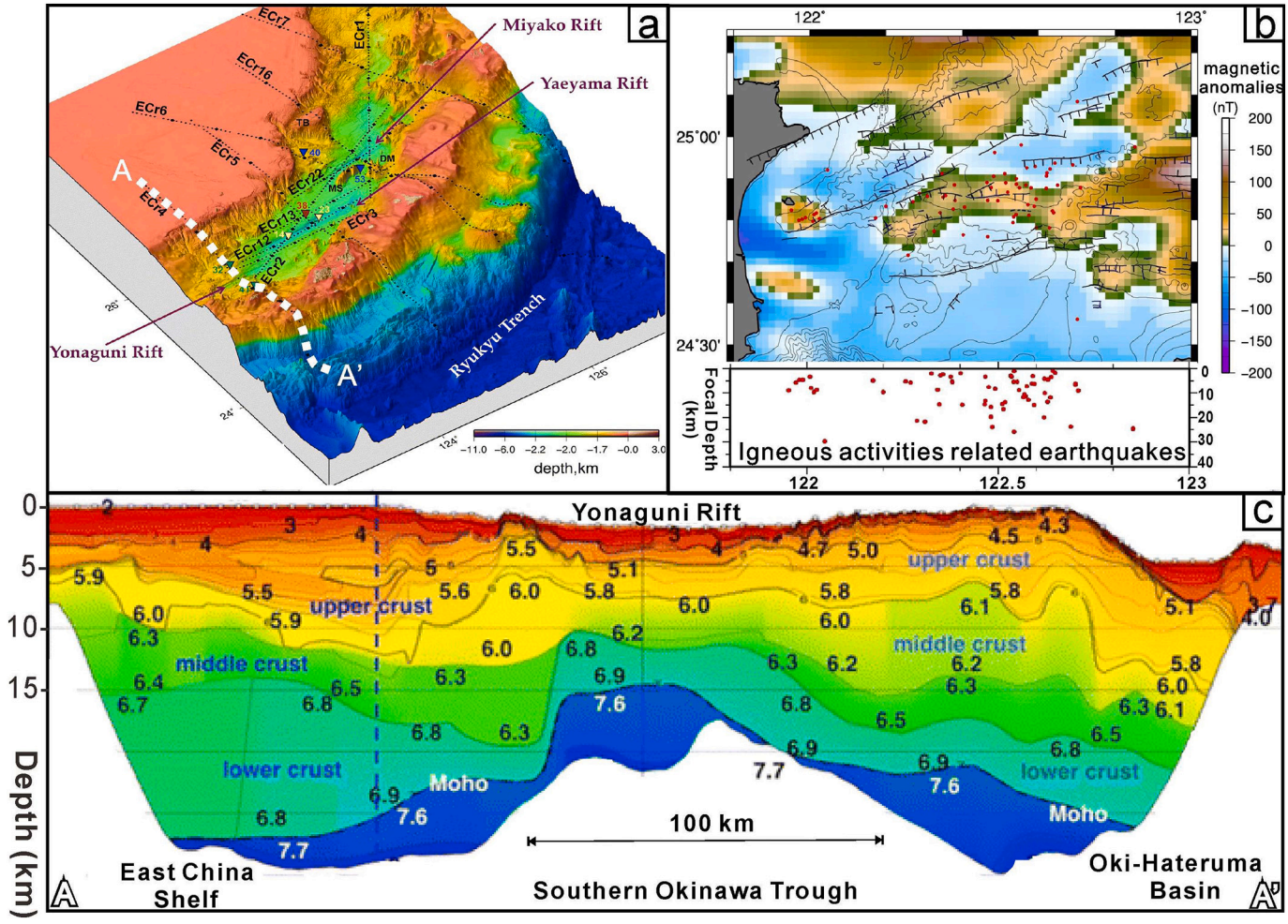

Fig. 2. Previous geophysical evidence of numerous igneous activities in SOT. (a) The locations of the igneous activities related to earthquakes are consistent with the magnetic anomalies, which are mostly shallower than 20 km and concentrated at the central axis of SOT (Sun, 2016). (b) Combining the seismicity with the profile images and Vp models derived from the numerous reflection and refraction seismic data, (c) the Vp model of the ECr4 profile along 123°E at YR suggests that there is high velocity attenuation at 5–10 km, which is related to the volcanic intrusion while crustal thinning (25 to 15 km) is currently in progress along the entire SOT. (Nishizawa et al., 2019).

earthquakes. Base on this approach, 67 volcano-related earthquakes are defined and consistent with the observation of magnetic anomalies (Hsu et al., 1998), which verify the shallow igneous activities (20 km) concentrated occur at the central axis of SOT (Sun, 2016) (Fig. 2c).The most remarkable hydrothermal venting field in the SOT, named Yonaguni Knoll IV (YK4), is situated at the southwestern tip of a NE-SW trending volcano trail of YR (Fig. 1), which might have originally developed through the subduction of the Gagua Ridge on the Philippine seafloor in the early Pleistocene (Sibuet et al., 1998). The YK4 hydrothermal system consists of four active hydrothermal fields, increasing temperature from the south (Mosquito Chimney, 163 °C) to the north (Lion, Tiger Chimneys, 328 °C), aligned with an approximately 1000 m-long and 500 m-wide, NNW–SSE trend linear depression fault system that controlled the fluid pathways to the seafloor (Suzuki et al., 2008). The biogeochemical and geochemical studies near YK4 detected liquid CO_2 and diverse microbial communities on the seafloor with black smokers originating from the intense hydrothermal activities (Nunoura and Takai, 2009). Previous studies reveal that focused investigation is necessary; especially the geophysical seafloor observations suggested that there are diverse hydrothermal convection schemes in the SOT (Masaki et al., 2011). Therefore, we designed dense seismic and heat flow surveys after capturing various flare images around GLM, to understand the fluid migration patterns by analyzing the regional structures with temperature fields to see if the volcano trail of YR could affect the hydrothermal system in this area.

3. Data and methodology

The latest field measurements around GLM were acquired by using the Violin-type or so-called “Lister-type” heat probe (HR-3), which was developed by the Institute of Oceanography at the National Taiwan University in cruises OR1-1175 and OR1-1205 in 2017 and 2018, respectively. The heat probe is 6 m in length, weighs 800 kg, and is equipped with 12 temperature sensors in a 1-cm diameter tube (right of Fig. 3), allowing for a resolution up to 0.1 mK (Shyu and Chang, 2005; Wu et al., 2019). This Lister-type marine heat probe can penetrate to seafloor sediments and simultaneously obtain the in-situ thermal gradient and the conductivity for calculating in-situ heat flows. Equipped with the Ultra Short Baseline (USBL) system and pre-calibration temperatures with records of the conductivity-temperature-depth (CTD), precise locations and bottom water temperatures can be derived. A typical temperature record for one of the thermistors installed with equal spacing down the probe consists of three distinct stages according to the status of heat probe penetration (Fig. 3). Before penetration of the sediment in the first stage, the temperatures recorded in the water can be used for the calibration of each sensor. The secondary stage is the thermal decay caused by frictional heating during penetration. The last but most important stage is another noticeable thermal decay of an instantaneous temperature rise caused by an artificial heat pulse generated from the instrument (Fig. 3), which is a critical temperature curve that yields the thermal conductivities through a least-squares best fit to the cylindrical decay function (Lister, 1979; Shyu and Chang, 2005).

Note that a previous well-known data reduction scheme of heat-flow that has been implemented is the two-step alternating iteration algorithm (Hartmann and Villinger, 2002; Shyu and Chang, 2005). The rationale behind this algorithm might be the intuition that one should increase the data constraints and downsize the model parameters to deal with an ill constrained non-linear inverse program. The temperature measurements of the sediments are much warmer than the surrounding seawater and cause an ambiguous frictional phase, which has also occurred in other hydrothermal venting sites (Hartmann and Villinger,

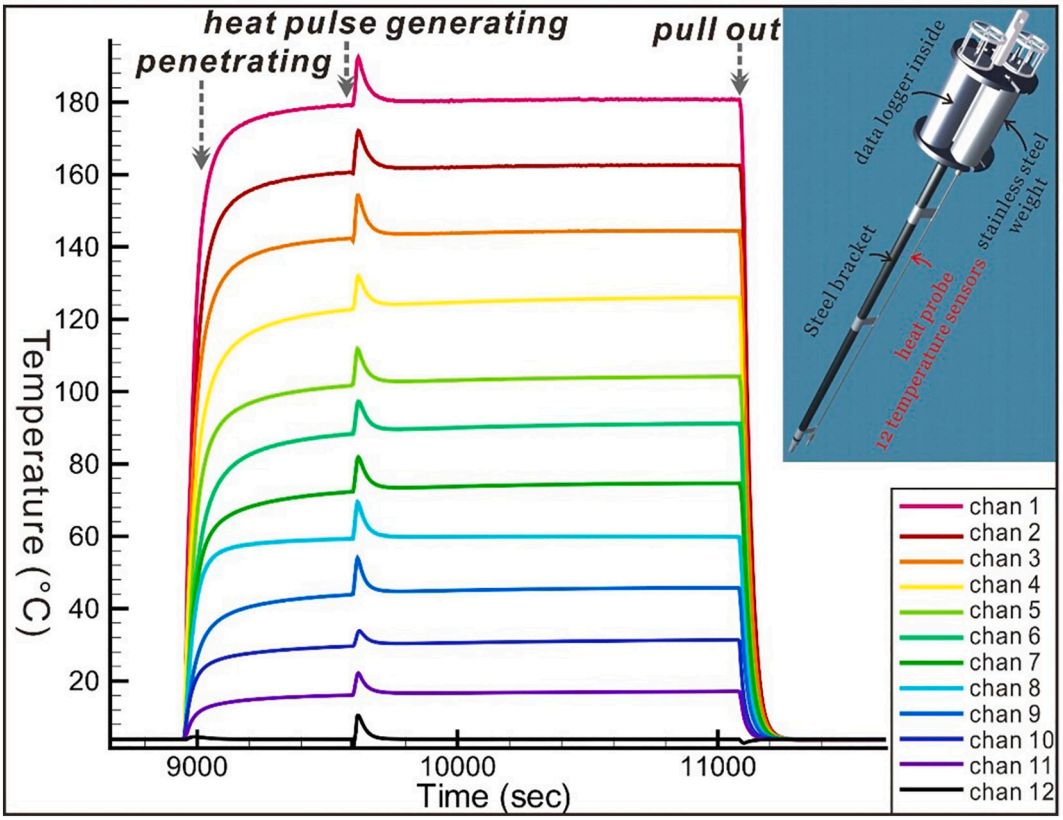

Fig. 3. Instrument introductions and the temperature records we derived in GLM. The Lister-type heat probe is equipped with 12 temperature sensors in a 1-cm diameter tube, the temperature records consist of three distinct stages according to the status of heat probe penetration: before penetrating, and thermal decays by the frictional heating during penetration and an artificial heat pulse generated from the instrument.

2002). Therefore, Wu et al. (2019) updated the heat-flow data reduction scheme by inverting essential thermal parameters to deal simultaneously with the same step of the temperature evolution from the pulse-heating, to avoid using the potentially ambiguous temperature evolution from the frictional phase. Based on this updated algorithm, robust estimations of the seafloor temperature measurements around the GLM have been rendered for further studies (Fig. 4).

The latest measured temperatures fields of these fifteen sites show a little departure from linearity generally (Figs. 4d and 5a), together with temperatures of the bottom water and seafloor, we can define the temperature gradients to estimate the heat flows (Fig. 4b) by multiplying the temperature gradients and thermal conductivities for each site (Table 1). However, the temperature profile detected at the G1 site, which is surrounding by fierce flares (Fig. 4c) (Tsai et al., 2019), reveals some discrepancies when it is compared with other sites (Fig. 5b). Therefore, we employed the ***Péclet number*** analysis based on an approach pioneered by Bredehoeft and Papadopulos (1965). Combining with the local physical properties, we can use our temperature profile to study the vertical fluid migration rate at G1 fluid conduit (Fig. 5b), similar to Wu et al. (2019a) and Chen et al. (2012). The ***Péclet number (β)*** may indicate the curvature representing the ratio of the rate of heat advection to the rate of conduction driven by an appropriate thermal gradient (Eq. (1)), while the concave direction was dominated by the upward or downward vertical fluid migration.

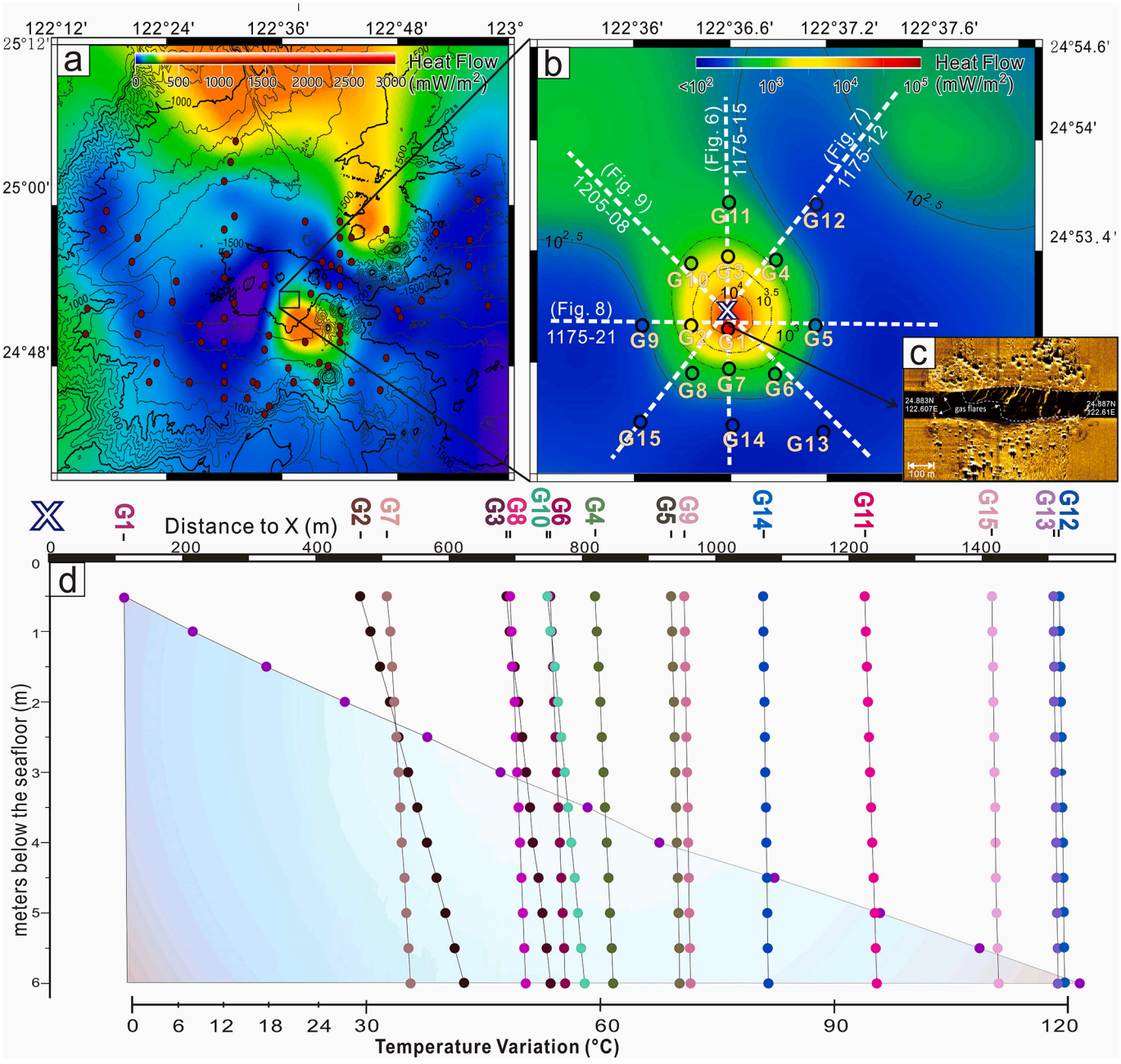

Fig. 4. Regional geothermal measured results at the GLM. (a) Previous heat flow observation results in the SOT (8–3000 mW/m^2) (Yamano et al., 1989; Shyu and Liu, 2001; Gutscher et al., 2016; Liu et al., 2016; Wu et al., 2019). (b) Our latest centralized measurements around GLM are represented by logarithm. (c) The clear images of the gas plumes in the water columns of deep-tow side scan sonar data. (d) Temperature variations against to depths and distances to central (X) of GLM display the enormous temperature anomaly at the G1 site.

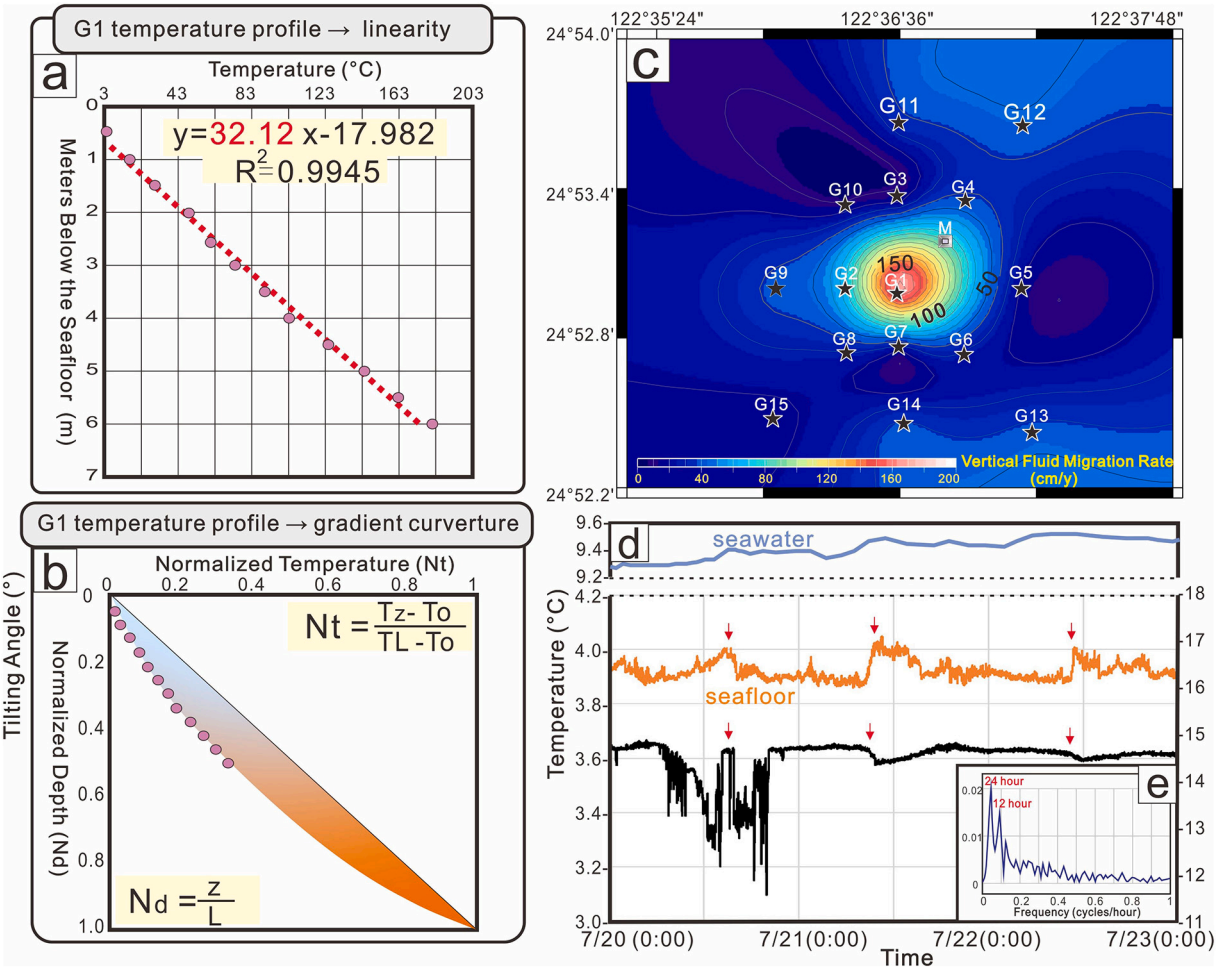

Fig. 5. Space and time evidence of the focus fluid flow. (a) The temperature gradient is about 32.12 K/m if we regarded the G1 temperature field as linearity. (b) The vertical fluid migration rate is about 185 cm/year if we regarded the G1 temperature field as a curvature. (c) The space distribution of the vertical fluid migration rates estimated from the ***Péclet number*** analysis by fitting the measured temperature variation patterns. (d) Time-dependent temperature variation in three days derived from small heat probes attached on the mooring instrument, the location of the instrument was situated at the "M" site, the red arrows indicate the possible fluid eruptions with temperature increases (~ 0.1 °C) while the tilting (~3°) occurred. (e) The Fast Fourier Transform (FFT) of the time series temperatures indicate the major periods of the temperature anomalies are 12 and 24 h. (For interpretation of the references to colour in this figure legend, the reader is referred to the web version of this article.)

$$\frac{T_z - T_0}{T_L - T_0} = \frac{e^{\frac{\beta z}{L}} - 1}{e^{\beta} - 1} \quad (1)$$

where $\boldsymbol{T_0}$ = the temperature at the top of a porous and permeable layer (seafloor) (°C);$\boldsymbol{T_L}$ = the temperature at the bottom of the porous and permeable layer (°C);$\boldsymbol{T_Z}$ = the temperatures we measured (°C);**z** = the subbottom depths we measured the temperatures (m);L = thickness of the porous layer (m), assuming it is a homogenous porous layer;ß = the Péclet number for the homogenous porous layer.

The normalized temperatures (***Nt***) and depths (***Nd***) display the best fitting curvature with the temperature profile to define the ***Péclet number (ß)*** (Fig. 5b).

$$Nt = \frac{e^{Nd} - 1}{e^{\beta} - 1} \quad (2)$$

The $\boldsymbol{\beta}$ allows us to calculate the vertical fluid velocity in the porous layer (Beardsmore and Cull, 2001) by using the Eq. (3) and Eq. (4). Here we calculate the upward fluid velocity of the GLM hydrothermal vent (Fig. 5c) by importing the depth-dependent temperatures and physical properties detected from the local core samples:

$$\beta = \frac{\varphi \rho_w c_w v_z L}{\lambda_r} \quad (3)$$

$$v_z = \frac{\varphi \rho_w c_w \beta L}{\lambda_r} \quad (4)$$

where $\boldsymbol{V_z}$: vertical fluid velocity of the fluid migration (cm/year);$\boldsymbol{\lambda_r}$: thermal conductivity of the porous medium (W/mK);$\boldsymbol{\varphi}$: porosity of the rock (%);ρw: density of the fluid (kg/m3);cw: the thermal capacity of the fluid (J/kgK);L: the thickness of the porous layer (m), assuming it is a homogenous porous layer.

Furthermore, we continually monitored the hydrothermal activities around the GLM by attaching two small temperature loggers on a mooring instrument to record the temperature variation of the seafloor sediments and bottom seawater (~ 1.5 m above the seafloor) with a 1-min sample interval (M site of the Fig. 5c) during a 3-days cruise (OR1–1202) in the summer of 2018. Combining with the oscillations documented by the tiltmeter, the continual temperature data record can report time-dependent hydrothermal activities of the GLM (Fig. 5d).

Besides, the regional seismic and chirp sonar images collected on R/V Ocean Research I (ORI) in 2017 and 2018, processed by the Ocean Center, National Taiwan University, may depict the subsurface structures with possible fluid migration pathways to joint interpret with corresponding heat flow observations (Hsu et al., 2019; Lin et al., 2019). The four critical directions of the seismic profiles were carried out for

Table 1
The latest heat-flow measurements collected around GLM in this study.

Site	Longitude	Latitude	WD	K	G	Q
	°N	°E	m	Wm^{-1} K^{-1}	K/m	mW/m^2
G1	122.610	24.883	1508	0.98	32.12 ± 6.134	31,477.6 ± 6.01
G2	122.606	24.883	1518	0.75	3.461 ± 0.148	2597.8 ± 0.11
G3	122.610	24.890	1507	1.21	1.49 ± 0.016	1804.78 ± 0.02
G4	122.615	24.889	1516	NaN	0.61 ± 0.035	NaN
G5	122.619	24.883	1508	1.09	0.29 ± 0.048	316.37 ± 0.05
G6	122.615	24.879	1512	NaN	0.511 ± 0.012	NaN
G7	122.610	24.879	1517	1.07	0.77 ± 0.114	819.22 ± 0.12
G8	122.606	24.879	1516	1.11	0.525 ± 0.025	582.2 ± 0.03
G9	122.601	24.883	1515	1.17	0.213 ± 0.012	248.9 ± 0.01
G10	122.606	24.889	1516	1.08	1.236 ± 0.055	1334.6 ± 0.06
G11	122.610	24.894	1508	1.22	0.41 ± 0.038	496.41 ± 0.05
G12	122.619	24.894	1518	1.14	0.179 ± 0.016	204.1 ± 0.02
G13	122.620	24.874	1510	NaN	0.154 ± 0.012	NaN
G14	122.610	24.874	1507	1.00	0.18 ± 0.029	180.7 ± 0.03
G15	122.601	24.875	1515	NaN	0.191 ± 0.084	NaN

WD = water depth, K = thermal conductivity, G = temperature gradient, Q = heat flow.

detail studying the geometry fluid conduit of GLM. Using the ProMAX seismic data processing software, the multi-channel seismic data were applied the trace editing, geometry building, bandpass filtering, amplitude compensation, predictive deconvolution, spiking noise removal, velocity analysis, normal move-out correction, trace balance, stacking, water velocity F-K time migration, and water column mute. The airgun array equips with 415 cubic inches source in total and the 120-channel long streamer (up to 1.5 km) allows us to image the subsurface structures deeper than 1 km. Moreover, the Bathy-2010p chirp sonar data were also acquired underway to observe the potential fluid conduit and to image the seafloor characteristics.

4. Results

Fifteen temperature measurements were conducted at depths to calculate the heat flow distribution around the GLM (Fig. 4a). Assumed the "X" point as the center of GLM, temperature gradients sharply decreased as the sites' distance to the "X" increased, from 32.12 K/m (G1) (Fig. 5a) to 0.15 K/m (G13) (Fig. 4c), implying the fluid migration induced by the hydrothermal activity of G1 fluid conduit. Meanwhile, eleven thermal conductivities were derived by fitting the temperature curves of the last stage to express well the constraints and constants for a given depth interval through the penetration depth. Except for four failed results due to malfunctions in the heat pulse generation (given 1.0 W/mK to infer the heat flow distribution), most thermal conductivities were successfully derived. Note that, two relatively lower thermal conductivities (0.75 and 0.98 W/mK) around the GLM were collected from the center of the GLM (sites G1 & G2), while the majority of the observations are larger than 1.0 W/mK (Table 1). As a result, the highest heat flow observation is up to 31,477.6 mW/m^2 at the G1 site demonstrates that intense hydrothermal activities around the GLM (Table 1), which is unrevealed from previous general heat flow surveys. (Fig. 4a) (Gutscher et al., 2016; Liu, 2018; Shyu and Liu, 2001; Yamano et al., 1989).

This latest heat flow survey also demonstrates the local thermal pattern by the focus distribution of the upward fluid velocities, which implies the conspicuous ascension of the fluid migration at the G1 site. After defining the possible depths and temperatures of the porous layer by trial and error, the vertical fluid velocities were estimated from the ***Péclet number*** analysis by fitting the measured temperature variation patterns (Bredehoeft and Papaopulos, 1965; Chen et al., 2012). Vertical fluid velocities at G1 and G2 are up to 185 and 75 cm/year, while others are ranging between 18 and 48 cm/year (Fig. 5c). Besides, the 3-day continuous temperature record successfully captured the potential fluid eruptions corresponding with the temperature increases (~ 0.1 °C) while the tilting angles (~ 3 °C) occurred (red arrows in Fig. 5d), and the Fast Fourier Transform (FFT) of the time series temperatures indicate the major periods of the temperature anomalies are 12 and 24 h (Fig. 5e). As we observed above, the time and spatial temperature fields suggest that the hydrothermal activity around the G1 site manifestly affect the thermal pattern of the GLM.

Here we extrapolated the temperature field to 25 m below the seafloor (mbsf) to cross-reference between temperature fields and the chirp sonar images since the chirp sonar profiles are capable to image the subsurface structures similarly (Figs. 6a to 9a). Through interpreting the observation of multiscale structures from seismic and chirp sonar profiles, we then speculate the possible development of the GLM hydrothermal vent by analyzing potential geological processes. 5. Interpretations.

The temperature of the G1 site is up to 181 °C at 6 mbsf implies it could exceed 300 °C at 9 mbsf (Figs. 6a to 9a); and the concentrations of Cl^- and Mg^{2+} in porewater decrease with depth whereas the total alkalinity increase indicates the phase separation of G1 hydrothermal fluid (Su, 2019). They both suggest the hydrothermal fluid might be mixing with the magmatic components according to the classification analyzed from the ascending hydrothermal fluids linked with the magma bodies with wider details (Fig. 10) (Kimura, 1985). Besides, a few temperature anomalies were found at the neighboring sites of G2 and G4 (Figs. 7a & 8a) while the high $^3He/^4He$ ratios (7.45 to 7.62 RA) observed in porewater samples (Su, 2019), displaying the significant signal of hydrothermal fluid as well. Combining the temperature fields with the chirp sonar images in subsurface sections, the temperature fields discernibly quench when the sites are distant from the G1 fluid conduit (Fig. 6a).

Different geophysical data illustrate the hydrothermal structures of the GLM differently. The profile sections present numerous fluid escape pipe structures in diverse scales (Figs. 6 to 9). With little seafloor variation (1500 to 1520 m water depth) at the GLM, the deep-tow side scan sonar images a 0.3-km^2 mounded structure while the area is reducing from northwest to southeast, and the vertical sections detected by the chirp sonar image about 0.16-km^2 acoustic blanking area of the G1 fluid conduit (the width are between 400 and 900 m from Figs. 6a to 9a). Furthermore, the hydrothermal vent complexes recognized from the multichannel seismic (MCS) profiles illustrate the G1 fluid conduit possibly span to 3800-m width at 3.1 s two-way travel time (TWTT) in the upper sediments of the SOT rifting basin (Fig. 6b).

After recognizing the morphology of the fluid conduits, faulting structures, and the fluid escaping pipes from each profile section (Figs. 6 to 9). Two zones of *E*-W directional faults observed in the North and South of GLM are diminishing toward the center, respectively; the symmetrical G1 fluid conduit along the N-S direction (Figs. 6b and 7b) corresponds with the regional crustal stress azimuth and the spreading direction of the SOT backarc basin (Gao et al., 2008; Wu et al., 2019) (Fig. 1a). Numerous fluid escape pipes emerge in the basin which indicates the fluid leakage at a porous permeable layer above the high-amplitude igneous reflections (blue arrows of Figs. 6b to 9b). In the vicinity of the GLM, the fierce fluid disturbance within the sediments along the G1 fluid conduit might indicate recent hydrothermal activities

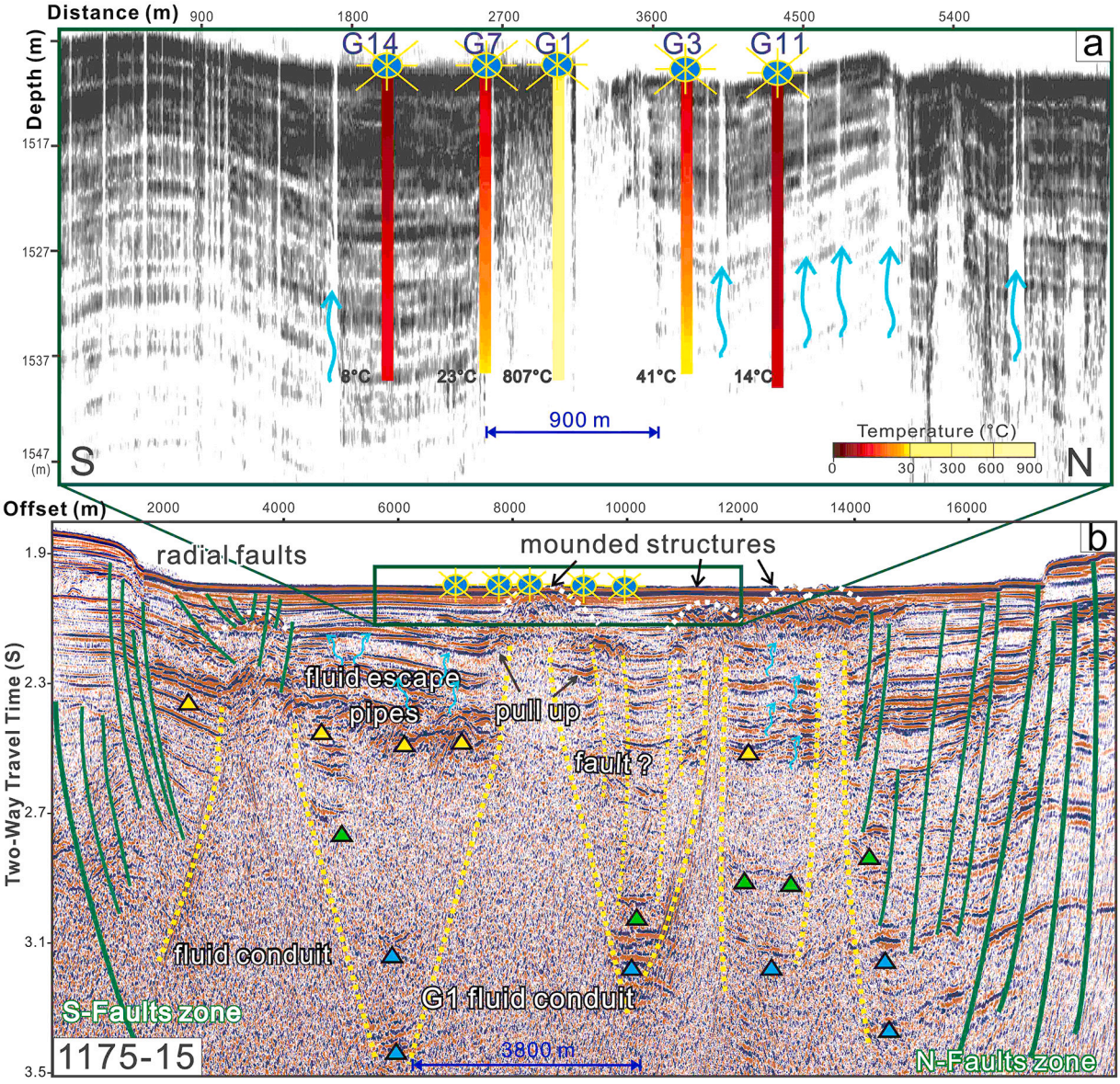

Fig. 6. Temperature variations and subsurface structures along 1175–15 profile in N-S direction. (a) The chirp sonar image combines with the temperature observation within 25 mbsf indicates that the ultrahigh temperature at the G1 fluid conduit may up to 807 °C at 25 mbsf; the width of the G1 fluid conduit is about 900 m in N-S direction. (b) The interpreted seismic profile illustrates the sedimentary basin strongly disturbed by the intrusive activities and fluid migrations. The possible width of the G1 fluid conduit at 3.5 TWTT is about 3800 m in N-S direction. The yellow triangles represent the bottom boundary of the fluid leakage within a permeable layer; the green triangles as the climbing saucer-shaped sills distinguished from the previous intrusions the concordant high amplitude reflections implied by the blue triangles might represent the sills with low-permeability units to constrain the upward fluid migrations. (For interpretation of the references to colour in this figure legend, the reader is referred to the web version of this article.)

while the pull up strata around the G1 fluid conduit suggest the successive vertical intrusive activities. Briefly, if N- and S- faulting zones impersonate the fluid migration pathways to allow the cold seawater infiltration into this rifting basin, thermal measurements did not cover this basin within these faults though, the development of a regional hydrothermal circulation could be achieved combining with other hydrothermal features.

The hydrothermal vent is a type of vertical columnar fluid flow feature corresponding with igneous intrusions; they are often characterized by a columnar conduit zone with disturbed and lowered acoustic reflections in seismic images. Due to the high fluid flux migration, hydrothermal vents are usually associated with sill complexes, starting at the tip of the sill intrusions and terminating in a characteristic upper part, which features as a dome or crater of the mound structures (Cartwright, 2007) (Fig. 6b). Planke et al. (2005) regarded the igneous sills as more significant parts of the volcanic plumbing systems, which substantially contribute to the lateral magma transport and storage at various levels in the Earth's crust, even though dikes are the main magma pathways from the lower crust to the Earth's surface. The high-amplitude igneous reflections corresponding to the possible presence of voluminous sill complexes are a discordant distribution, while the presence of voluminous sill complexes are regarded as the essential component of hydrothermal pumping systems in sedimentary basins (Magee et al., 2016; Planke et al., 2005; Svensen et al., 2012). Therefore, we identify three groups of the high-amplitude reflections from the MCS profiles, including the possible igneous depositions or sills that possess local transgressions or abrupt terminations, to study the potential thermal pattern around GLM (Figs. 6b to 9b):

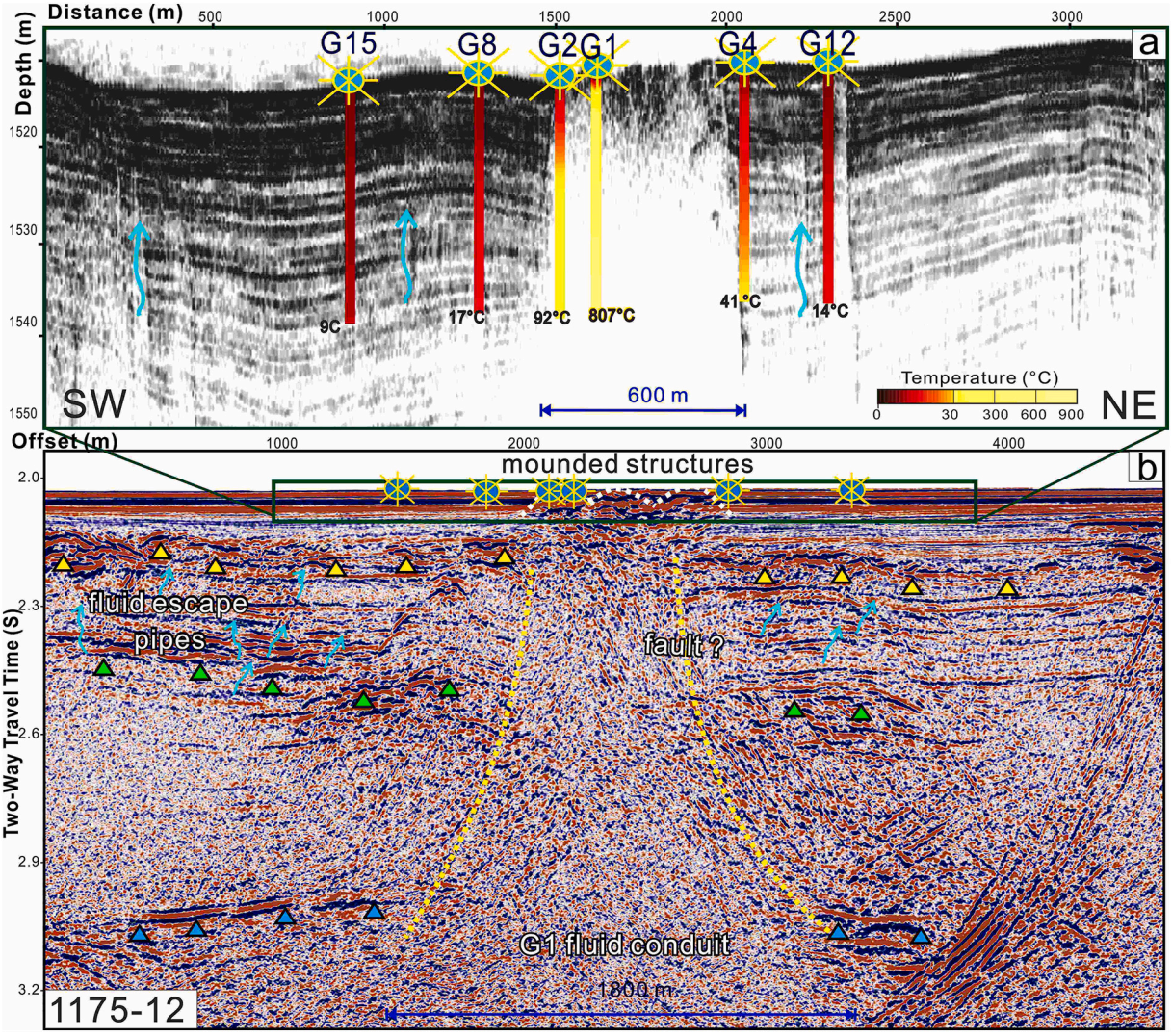

Fig. 7. Temperature variations and subsurface structures along 1175–12 profile in NE-SW direction. (a) The chirp sonar image combines with the temperature observation within 25 mbsf indicates that the ultrahigh temperature at G1 fluid conduit vigorously affects G2 and G4 sites as well; the width of the G1 fluid conduit is about 600 m in NE-SW direction. (b) The convex reflections around the fluid conduits might suggest previous hydrothermal events with the sprawling igneous units, and the triangles are consistent with the aforementioned features. The possible width of the G1 fluid conduit at 3.2 TWTT is about 1800 m in NE-SW direction.

(1) At 2.2 to 2.4 s TWTT, the yellow triangles represent the bottom boundary (probable occurred as an eruptive vent) of the fluid leakage within a permeable layer while the dome-shaped mounded structures were observed near the seafloor with fluid intense disturbing below. They are possible layer parallel and planer transgressive sills in N-S (Fig. 6b) and E-W directions (Fig. 8b), respectively. Especially some inward-dipping or outward-dipping reflections around the fluid conduits (Figs. 7b and 8b) might indicate the latest hydrothermal events with the sprawling igneous units.

(2) At 2.4 to 3.0 s TWTT, we regard the green triangles as the climbing saucer-shaped sills distinguished from the previous intrusions by a deeper deposition level with a greater width of the saucers mainly in NE-SW direction (Fig. 7b). The convex reflections around the fluid conduits also indicate previous hydrothermal events with the sprawling igneous units (Fig. 7b), however, the signals are getting ambiguous when they are in N-S direction (Fig. 6b), which might metaphor the main eruptive direction is tending to NE-SW.

(3) At 3.0 to 3.3 s TWTT, the green triangles, the concordant high amplitude reflections implied by the blue triangles might represent the sills with low-permeability units to constrain the upward fluid migrations; they exhibit smooth layer parallel and planner transgressive facies in NE-SW direction (Fig. 6b) and SE-NW direction (Figs. 7b and 8b).

Briefly, we regard these irregular high amplitude reflections as the sill structures at different permeability layers of the sedimentary basin. Thus, some small areas in Fig. 6 with magnetization lows could reflect the characteristics of shallow subsurface materials and ions (triangles of Figs. 6b to 9b) are accordant with the hydrothermal events and the layering of the host rock (Jackson et al., 2013), which has emplaced the sills-feeding-sills sedimentary basin at an undetectable depth of this basin (Airoldi et al., 2016; Galland et al., 2018). Moreover, the earthquakes associated with igneous activities had verified the shallow igneous activities (~20 km) concentrated occur at the central axis of SOT (Sun, 2016) (Fig. 2b). Moreover, the porewater analysis from the G1 gravity core, through the decrease Mg^{2+} and Cl^{-} and increase of total alkalinity, as well as the steadily high ratio of $^{3}He/^{4}He$ along the depth profile, convincingly demonstrate the phase separation reaction of hydrothermal activities and fluid upward migration at site G1 (Su, 2019). Hence, it is conceivable that the shallow igneous activities supplied the

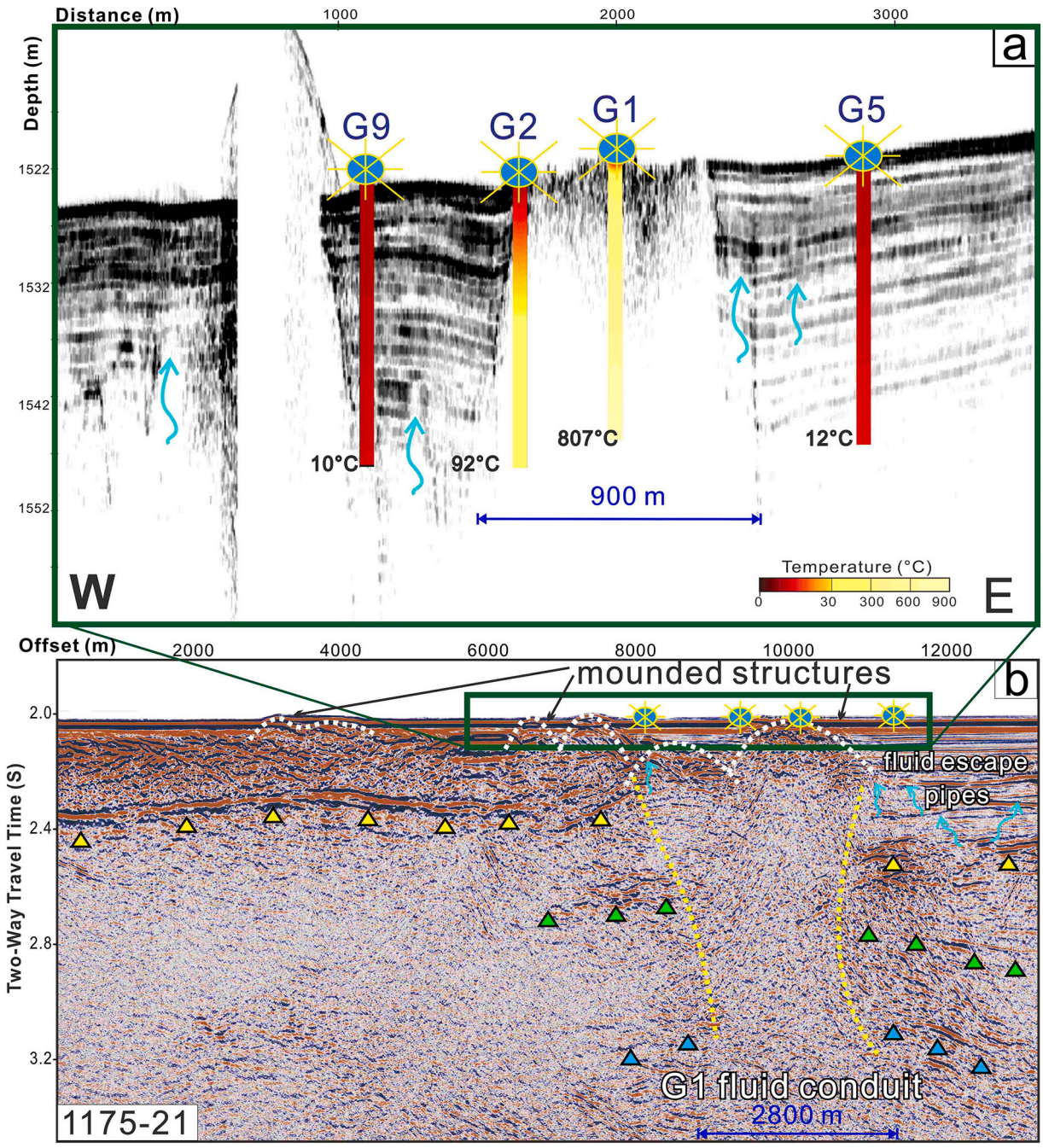

Fig. 8. Temperature variations and subsurface structures along 1175–21 profile in E-W direction. (a) The chirp sonar image combines with the temperature observation within 25 mbsf emerges that the temperature anomaly sharply eases once they leaving away the G1 fluid conduit; the width of the G1 fluid conduit is about 900 m in E-W direction. (b) The interpreted seismic profile recognizes a layer parallel high-amplitude reflections (~2.35 TWTT) that may extend to the west to allow the lateral fluid migration above it, and the triangles are consistent with the aforementioned features. The possible width of the G1 fluid conduit at 3.2 TWTT is about 2800 m in E-W direction.

GLM hydrothermal vent to develop the sills-feeding-sills sediments as an igneous province and caused the enormous heat anomaly at the G1 fluid conduit.

5. Discussion

5.1. Regional thermal model in the SOT

Previous measurements of the thermal conductivities in the SOT ranged approximately between 1 ± 0.25 W/mK which are similar to the typical marine sediments (Lu et al., 1981; Shyu and Liu, 2001; Wu et al., 2019). The two highest heat flow observations (sites G1 and G2 at the central of GLM) with the lowest thermal conductivities (0.75 and 0.98 W/mK) suggested the measurements were disturbed by the fierce flares while the thermal conductivities of most minerals may decrease with the rising temperatures (Balling et al., 1981; Demongodin et al., 1991). However, the highest heat flow with the highest thermal conductivity (1.36 W/mK) at a neighboring hydrothermal field YK4 (Wu et al., 2019) suggested there are a considerable amount of sulfide-bearing sediments deposited from the hydrothermal vent fluid, which is consistent with the in-situ geochemical observation at YK4 (Su, 2019) and the observation at the Jade site of the MOT (Kinoshita and Yamano, 1997).

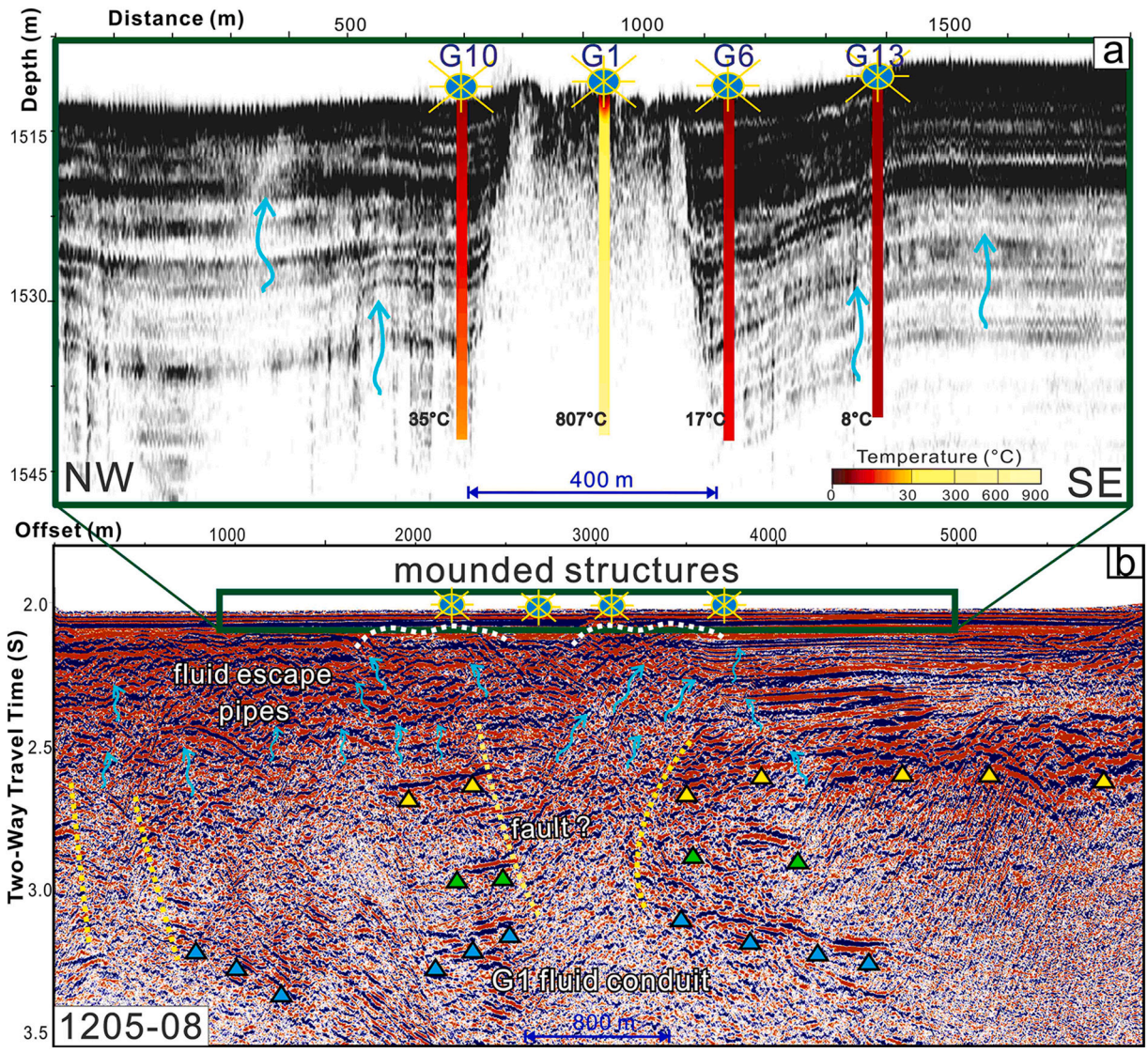

Fig. 9. Temperature variations and subsurface structures along 1205–08 profile in SE-NWdirection. (a) The chirp sonar image combines with the temperature observation within 25 mbsf illustrates that the ultrahigh temperature occurs at the center of the G1 blanking zone, while the width of the G1 fluid connduit is reducing to 400 m in SE-NW direction; (b) The interpreted seismic profile recognizes numerous fluid escape pipes emerge in the basin which indicates the fluid leakage at a porous permeable layer above the high-amplitude igneous reflections. The triangles are consistent with the aforementioned features, and the possible width of the G1 fluid conduit at 3.2 TWTT is about 800 m in NW-SE direction.

For the higher heat flow observations at the SOT, Watanabe et al. (2006) regarded that they indicated the shallow heat sources associated with the recent arc expanding activity, while Shyu and Liu (2001) suggested them as the local fluid circulation possibly influenced by the adjacent volcanic centers. Suzuki et al. (2008) had interpreted that faults can provide the fluid migration pathways to the seafloor while the high but variable heat flows and nonlinear temperature gradients in the depression are taken to indicate a high level of hydrothermal activity (Kinoshita et al., 2006). At the YK4 of the SOT, a heat flow contrast of more than 3000 mW/m^2 within a short distance (~ 1 km) implies the active hydrothermal circulation locally (Gutscher et al., 2016; Shyu and Liu, 2001; Yamano et al., 1989). Moreover, at the GLM of the SOT, we had observed a heat flow contrast of more than 28,000 mW/m^2 within 300 m (Fig. 4), the venting mechanism of the buoyancy forces should be considered here, while the hydrothermal fluid upward migration is thought to be driven by magmatic sources (Sakai et al., 1990).

On the contrary, numerous sediments may vary the thickness of the depocenter and reduce the in-situ heat flow, thus, the cooling effect caused by the subsidence of the sedimentary basin in the SOT also needs to be considered (Turcotte and Ahern, 1977). The heating of pore fluids in the sedimentary sequences may be caused by the burial process before the initiation of metamorphism, whereby the low-temperature hydrothermal fluid circulation can occur in the basins (Right of Fig. 10) (Sharma and Srivastava, 2014). Usually, the high heat flow measurements appear close to the hydrothermal venting sites, whereas the low measurements are associated with the seawater charging sites (Fisher et al., 2003). Previous heat flow surveys regarded the SOT as a cold sedimentary basin with some local focus heating effect caused by some obvious hydrothermal system (Fig. 4a) (Shyu and Liu, 2001), in recent studies, ultrahigh temperatures (Fig. 4d) with the phase separation reaction of hydrothermal activities (Su, 2019) at the GLM indicate the existence of shallow magmatic components to dominate the ascending hydrothermal fluids to cause a focus heating effect (Fig. 10a). Integrating our focus observation with the large-scaled hydrothermal circulation system of the SOT suggested by Shyu and Liu (2001), a conceptual model has been proposed to represent the thermal model from the heat flow observation of the SOT (Fig. 11). Heat flow measurements primarily reflect the conductive heat flow; the missing heat

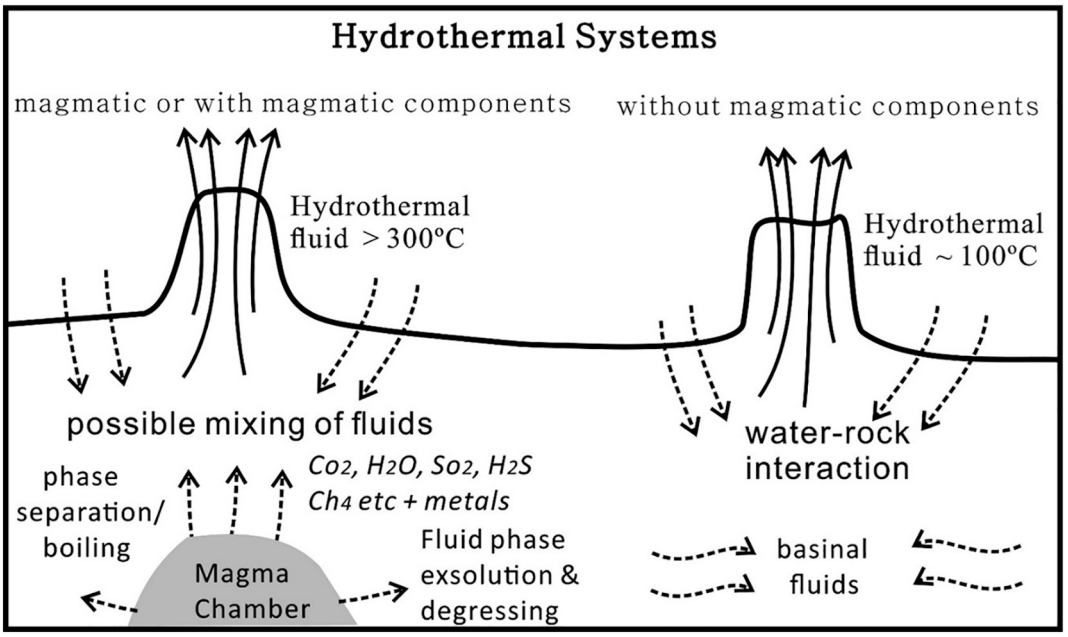

Fig. 10. Hydrothermal fluid models may with or without magmatic components analyzed by the ascending hydrothermal fluids (Kumar & Singh, 2014). Here we adopt the hydrothermal fluid might be mixing with the magmatic components, base on our ultrahigh temperature observation at GLM.

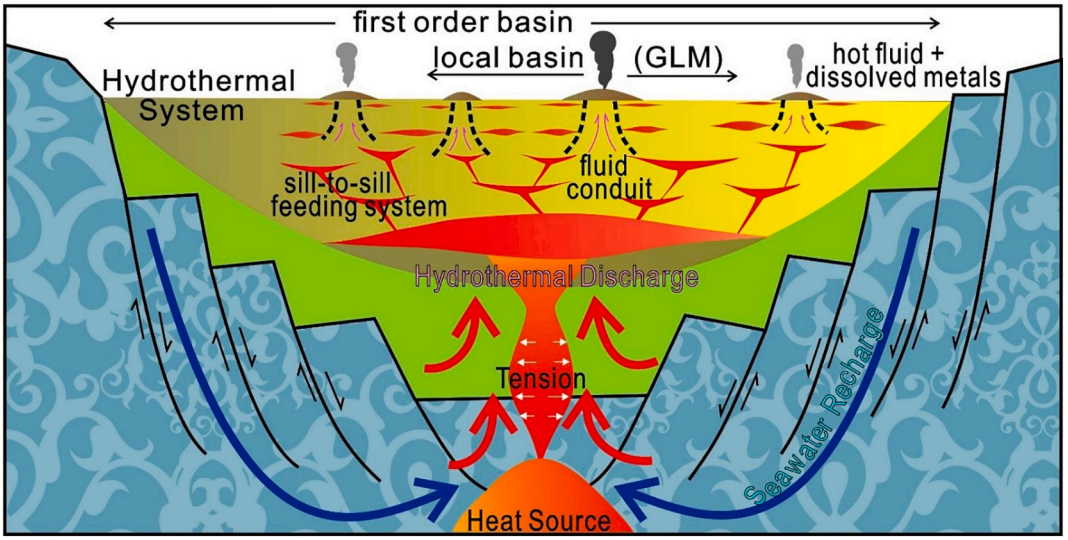

Fig. 11. The geological thermal model of the SOT. Our schematic model illustrates the possible sill-to-sill feeding sedimentary basin, with the cold seawater (blue-dashed arrows) supplied from the N and S fault zones and heated by the magnetic heat source as the hydrothermal discharge, then sill-to-sill feeding the intrusive activities might be capable to drive the igneous materials to the shallow crust. (For interpretation of the references to colour in this figure legend, the reader is referred to the web version of this article.)

transported by convection must appear somewhere, either as high conductive heat flow or as an advective discharge to the sea (Stein and Von Herzen, 2001). The discovery of the focus fluid flow around GLM (Figs. 4 and 5) explicitly demonstrated the hydrothermal discharge supporting the high conductive heat propagation to the seafloor. Scheirer et al. (2006) suggested the temperature variation within a diffuse flow field often varied by 5–10 °C and synchronous with near-bottom currents dominated by tidal and inertial forcing, nevertheless, our time-dependent temperature variations in three days (Fig. 5d) may be also dominated by the Diurnal or Semi-diurnal tidal effect as well (Fig. 5e). It denotes that our limited duration of the temperature observation might not capture the crystal cracking events from deeper heat source but record the background heat spouts induced by the tidal forces regularly. Base on the ultrahigh temperature observed at site G1, the hydrothermal fluid of the GLM might be mixing with the magmatic components (Fig. 10) (Sharma and Srivastava, 2014).

Through the seismic interpretations, we recognized numerous sill structures from the seismic profiles around the GLM (Figs. 6b to 9b) to provide the shallow heat sources for delivering the heat from deeper magma chambers, while the sill-to-sill feeding system has been widely described as the resemble junctions between sills (Hansen et al., 2004). Our observation is similar to the example of the NE Atlantic margin, the vents formed at the palaeo-seabed as a result of sill intrusion and the vent fill ranges in composition from entirely remobilized sedimentary to dominantly magmatic (Hansen, 2006). And the wide occurrence of such junction sills was suggested that they were interconnected through sill-

to-sill feeding relationships at the time of their emplacement (Cartwright and Hansen, 2006). Therefore, our conceptual model indicates the GLM as a major recharge zone to diffuse the flow vents and exhibit much greater temperature variability than adjacent hydrothermal vents; furthermore, it may indicate the volcano trail of YR could affect the hydrothermal system of the GLM. However, a general distribution of the temperature measurements can better illustrate the lateral fluid flow at subsurface with regionally nearly isothermal effect (Scheirer et al., 2006, since we only have the focus the large-scaled heat flow observation (Shyu and Liu, 2001) in this study.

5.2. Fluid circulation of the GLM

The simplified sketch exhibits the evolution of hydrothermal fluids in a geologically active site; cold seawater entrains the fractured crust, heats up and reacts with the rock in the reaction zone, and then flows up again as hot hydrothermal fluid to the seafloor (Fig. 11). For the fluid recharge, the first order basin was amplified by some tremendous faults situated at the north and south boundaries of the SOT backarc basin. The normal faults were recognized from the seismic profiles and might be affected by the vicinity of the hydrothermal events to raise the local temperature field. Therefore, the sill-to-sill feeding sedimentary basin of the GLM is capable of demonstrating the enormous thermal anomaly around the spreading center of the SOT and representing the hydrothermal discharge with extremely high conductive heat along the G1 fluid conduit. Even though the deeper magma sources are still ambiguous from the observations, the temperature anomaly observed around the G1 fluid conduit concludes the existence of high conductive heat in the shallow sediments. Considering about the hydrothermal vent circulation pathways are restricted in a permeable channel, a detailed mapping to establish the 3D geometry of the full-scale hydrothermal circulation is the primary demand for proving the vertical and lateral dimension of the circulation cell, and other crucial factors are the well-distributed heat flow observations and focused material geochemistry analysis of the hydrate-bearing sediments. Different from the GLM, the isotopic alteration study provided a black smoker vent field along the mid-ocean ridges as a hydrothermal circulation around detachment faults evolves from basalt hosted (TAG type), to footwall ultramafic hosted (Rainbow type), to low-temperature ultramafic hosted (Lost City type). The key feature of this model is the intrusion of gabbro bodies immediately below the detachment to provide a heat source for circulation, and focusing fluid flow into the detachment fault to allow venting away from the new volcanic axis (McCaig et al., 2007), which is largely different with our conceptual model of the GLM.

Locations of where the seawater flows into the seafloor to recharge the hydrothermal cells within the crustal reservoir are by contrast almost invisible but can be indirectly identified by a systematic grid of conductive heat flow measurements. Johnson et al. (2010) had measured the conductive heat flow values from the thermal blanket experiment in Juan de Fuca Ridge and grouped results into three categories (Fig. 12b), after identified the recharge zones from an array of conductive heat flow stations in the Endeavour axial valley that appear to represent a nested system of fluid circulation paths (Fig. 12a). Therefore, combining previous thermal data with the latest measurement (Lu et al., 1981; Shyu and Liu, 2001; Wu et al., 2019), we imitated this strategy to roughly classify our heat flow results to three groups (Fig. 12c). Although the values of 140 and 20 mW/m^2 are somewhat arbitrary, a comparison to heat flows taken outside of the axial basin above sedimentary basin indicates that they are plausible limits to identify sources of fluid advection and recharge (Johnson et al., 1993). The regional heat flow distribution with distinct colour-bar to insinuate the possible recharge (red) and discharge (blue) zones around the GLM is consistent with the venting and faulting areas in the N-S direction, respectively (Fig. 12c). Thus, we simplify the 2-D, cross-axis model structure, from the seafloor to Moho geometry at this rifting basin to cartoon illustrate the small scale hydrothermal circulation, including the different permeable layer for hydrothermal convection, and the moho depth we defined from the magnetic and seismic data (Fig. 12d). The shallower permeable layer we recognize from the seismic profiles (above yellow triangles of Figs. 6b to 9b) represents the fluid leakage to support the lateral hydrothermal convection, and the Vp model and magnetization lows indicate the bottom of the layer with the sills structures to allow the upper crust convection (Fig. 12d).

5.3. The precious metals in the hydrothermal deposition

Hydrothermal fluids on the seafloor typically form by the circulation of seawater in the fractured oceanic, circulating seawater is heated by a heat source such as a magma chamber or associated hot rock and, during heating and chemical reaction with the surrounding rock, undergoes a suite of chemical modifications. Thus, hydrothermal fluid migration systems developed on the modern seafloor are important carriers of base and precious metals in a wide range of volcanic and tectonic settings. The concentrations and distribution, especially of gold and silver, in associated seafloor massive sulfide (SMS) deposits are strongly influenced by variable source rocks, fluid chemistry, and precipitation mechanisms. For example, the “Lena” chimney is a 2-m-high sulfide mound perched on a steep slope in Kermadec Arc, the vent fluid emanating from the top of the chimney had a maximum temperature of 274 °C, and the average gold concentrations in the chimney samples are 8.5 ppm (8500 ng/g) (de Ronde Cornel et al., 2011); at the GLM, the temperature of the G1 site had measured a maximum temperature of 181 °C at 6 mbsf, and extremely high concentrations of Ag, Zn, and Au were found in the seafloor sediments, which exceeded 140,00 ng/g, 10,000 μg/g, and 300 ng/g, respectively (Su, 2019). Recently, the compositional data of 130 SMS deposits around the world show a large range of gold and silver grades, Fuchs et al. (2019) recognized some complexity exists, such as mixing with cold seawater can shift the deposition or boiled silver precipitation limited by the conservative behavior of Cl^-, and that Au enrichment may be attributable to different processes in different deposits has important implications for exploration.

6. Conclusion

Combining the latest geophysical surveys with the detailed thermal measurements around SOT, we interpreted the nature of the fluid conduits, the underlying sill complex, with the vertical temperature variations to analyze the subsurface thermal model. The latest heat flow measurements of the GLM illustrate a concentric heat flow reduction from 31,477 to 180 mW/m^2 at a 1-km distance surrounding the G1 site, which not only demonstrates the focus fluid migration along the G1 fluid conduit but also indicates that the ultra-high temperatures are related to the existence of the magmatic components in shallow sediments. Here we proposed a conceptual model to satisfy the observation of previous general surveys and current detailed measurements of the SOT. The simplified sketch exhibits the evolution of hydrothermal fluids in a geologically active site; cold seawater entrains the fractured crust, heats up and reacts with the rock in the reaction zone, and then flows up again as hot hydrothermal fluid to the seafloor. The sill-to-sill feeding sedimentary basin is capable to demonstrate the enormous thermal anomaly around the spreading center of the SOT and represents the hydrothermal discharge with extremely high conductive heat along the G1 fluid conduit. We also classify our heat flow results to the possible recharge and discharge zones and using a cross-axis model to represent the small scale hydrothermal circulation of the GLM. For the concentrations of the precious metals in the hydrothermal deposits, the temperature of the G1 site had measured a maximum temperature of 181 °C at 6 mbsf, and extremely high concentrations of Ag, Zn, and Au were found in the seafloor sediments, which exceeded 140,00 ng/g, 10,000 μg/g, and 300 ng/g, respectively. We had roughly defined the discharge and recharge zones of the hydrothermal circulations from our focus and previous

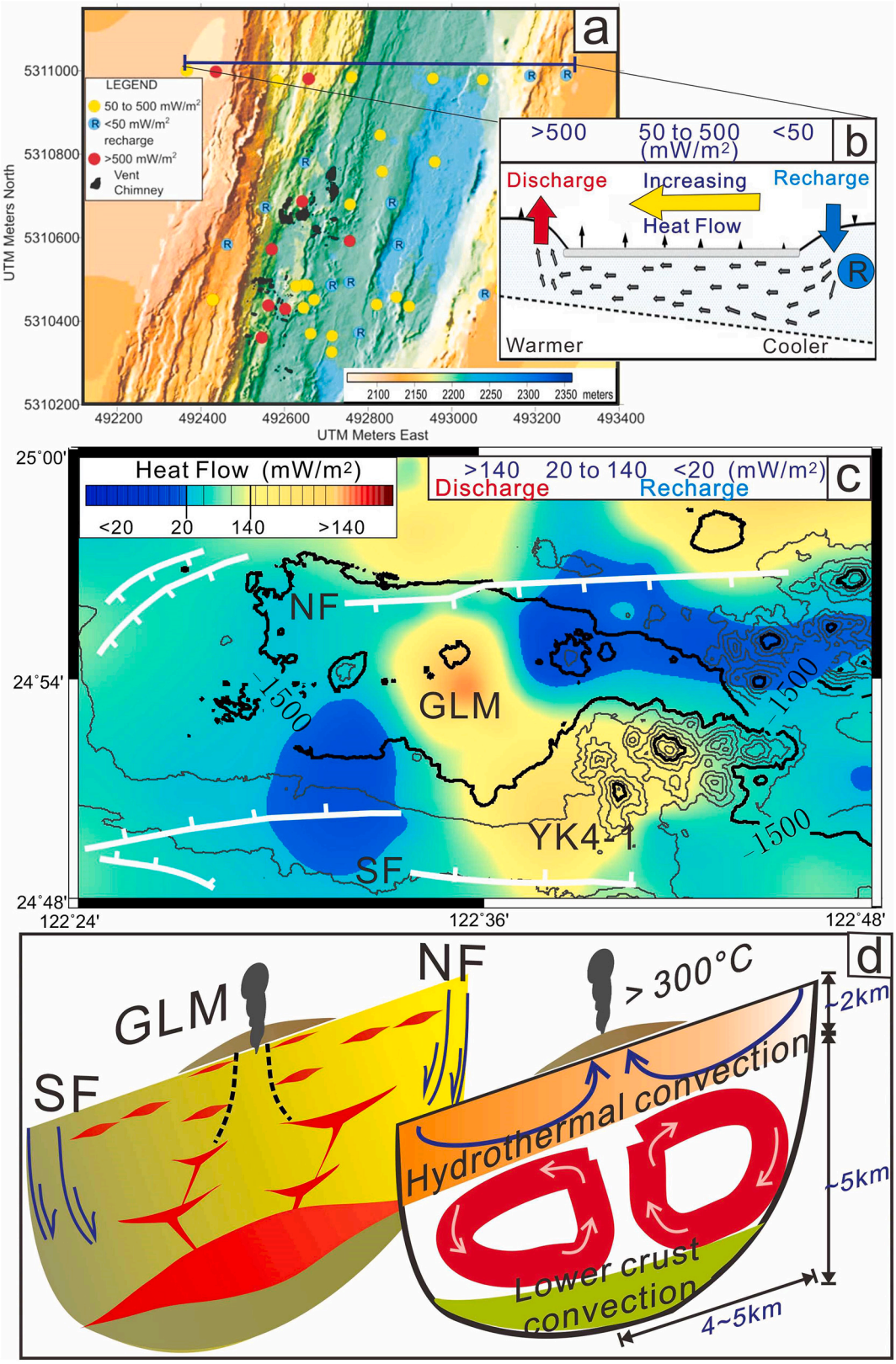

Fig. 12. The possible fluid circulation of the GLM. Colored circles correspond to recharge (blue), conductive (yellow), and discharge (red). (a) The recharge zones (circled R) measured by the thermal blanket stations in the Endeavour axial valley plotted on the bathymetry data (Johnson et al., 2010). (b) Interpretive cartoon of North Line heat flow data, with recharge occurring on the valley eastern boundary fault and lateral subsurface transport beneath the valley to discharge on the valley western boundary fault. (c) We imitated this strategy to roughly classify our heat flow results to three groups after combining previous thermal data with the latest measurement (Lu et al., 1981; Shyu and Liu, 2001; Wu et al., 2019). (d) *We* illustrate the small scale hydrothermal circulation including the different permeable layer for hydrothermal convection to represent the possible hydrothermal convection cross the axis. (For interpretation of the references to colour in this figure legend, the reader is referred to the web version of this article.)

general heat flow observation, The long-term monitoring of the hydrothermal activity cross the axis between the faulting zones will be another crucial feature we should discern, and the further physical properties and geochemical analyses are also needed to validate the whole hydrothermal structure of the SOT.

Credit author statement

Liwen Chen and Hsieh-Tang Chiang collected, analyzed, and joined the interpretation of the comprehensive dataset and propose the main idea. Jyun-Nai Wu collected and processed the heat flow data. Char-Shine Liu collected and calibrated the seismic dataset. Ling-Yun Chiao and Chuen-Tien Shyu assisted on the analysis of the heat flow data. Yunshuen Wang and Song-Chuen Chen helped the design of the manuscript including providing geological background information.

Declaration of Competing Interest

None.

Acknowledgments

We would like to acknowledge H.-Y. Chang for his contribution of building the recording system of the instrument. The marine geophysical data acquirement would not be achieved without the efforts of the crews and shipboard technicians of the R/V Ocean Research I and S. D. Chiou of the Ocean Research Precious Instrument Center, NTU. We are also grateful to the teamwork of the Seismic Exploration Laboratory of Ocean Center, as well as Professor Su's Environmental Radiology and Sedimentation Laboratory, NTU. This study is supported by the Central Geological Survey, Taiwan, MOEA grant 107-5226904000-05-01, as well as the grant of Ministry of Science and Technology, Taiwan, MS-105-2611-M-002-001-MY3.

References

Airoldi, G.M., Muirhead, J.D., Long, S.M., Zanella, E., White, J.D., 2016. Flow dynamics in mid-Jurassic dikes and sills of the Ferrar large igneous province and implications for long-distance magma transport. Tectonophysics 683, 182–199.
Balling, N., Kristiansen, J.I., Breiner, N., Poulsen, K.D., Rasmussen, R., Saxov, S., 1981. Geothermal Measurements and Subsurface Temperature Modelling in Denmark.
Bredehoeft, J.D., Papaopulos, I.S., 1965. Rates of vertical groundwater movement estimated from the Earth's thermal profile. Water Resour. Res. 1, 325–328.
Cartwright, J., 2007. The impact of 3D seismic data on the understanding of compaction, fluid flow and diagenesis in sedimentary basins. J. Geol. Soc. 164, 881–893.
Cartwright, J., Hansen, D.M., 2006. Magma transport through the crust via interconnected sill complexes. Geology 34, 929–932.
Chen, L., Chi, W.-C., Liu, C.-S., Shyu, C.-T., Wang, Y., Lu, C.-Y., 2012. Deriving regional vertical fluid migration rates offshore southwestern Taiwan using bottom-simulating reflectors. Mar. Geophys. Res. 33, 379–388.
Chouet, Bernard A., 1996. Long-period volcano seismicity: its source and use in eruption forecasting. Nature 380 (6572), 309–316.
Demongodin, L., Pinoteau, B., Vasseur, G., Gable, R., 1991. Thermal conductivity and well logs: a case study in the Paris basin. Geophys. J. Int. 105, 675–691.
Elderfield, H., Schultz, A., 1996. Mid-ocean ridge hydrothermal fluxes and the chemical composition of the ocean. Annu. Rev. Earth Planet. Sci. 24 (1), 191–224.
Fisher, A.T., Davis, E.E., Hutnak, M., Spiess, V., Zühlsdorff, L., Cherkaoui, A., Christiansen, L., Edwards, K., Macdonald, R., Villinger, H., Mottl, M.J., Wheat, C.G., Becker, K., 2003. Hydrothermal Recharge and Discharge across 50 km Guided by Seamounts on a Young Ridge Flank.
Fuchs, S., Hannington, M.D., Petersen, S., 2019. Divining gold in seafloor polymetallic massive sulfide systems. Mineral. Deposita 54 (6), 789–820.
Galland, O., Bertelsen, H.S., Eide, C.H., Guldstrand, F., Haug, Ø.T., Leanza, H.A., Mair, K., Palma, O., Planke, S., Rabbel, O., Rogers, B., Schmiedel, T., Souche, A., Spacapan, J.B., 2018. Chapter 5 - storage and transport of magma in the layered crust—formation of sills and related flat-lying intrusions. In: Burchardt, S. (Ed.), Volcanic and Igneous Plumbing Systems. Elsevier.
Gao, J., Zhang, T., Fang, Y., Yang, C., Mei, S., 2008. Faulting, magmatism and crustal oceanization of the Okinawa Trough. Acta Oceanol. Sin. 28 (3), 40–49.
Glasby, G.P., Notsu, K., 2003. Submarine hydrothermal mineralization in the Okinawa Trough, SW of Japan: an overview. Ore Geol. Rev. 23, 299–339.
Gutscher, M.-A., Klingelhoefer, F., Theunissen, T., Spakman, W., Berthet, T., Wang, T.K., Lee, C.-S., 2016. Thermal modeling of the SW Ryukyu forearc (Taiwan): Implications for the seismogenic zone and the age of the subducting Philippine Sea Plate (Huatung Basin). Tectonophys. Geodyn. Environ. East Asia 131–142. GEEA 2014 692.
Han, B., Zhang, X.-H., Pei, J.-X., Zhang, W.-G., 2007. Characteristics of crust-mantle in East China sea and adjacent regions. Prog. Geophys. 22, 376–382.
Hansen, D.M., 2006. The morphology of intrusion-related vent structures and their implications for constraining the timing of intrusive events along the NE Atlantic margin. J. Geol. Soc. 163 (5), 789–800.
Hansen, D.Mø., Cartwright, J.A., Thomas, D., 2004. 3D seismic analysis of the geometry of igneous sills and sill junction relationships. Geol. Soc. Lond. Mem. 29, 199–208.
Hartmann, A., Villinger, H., 2002. Inversion of marine heat flow measurements by expansion of the temperature decay function. Geophys. J. Int. 148, 628–636.
Hirata, N., Kinoshita, H., Katao, H., Baba, H., Kaiho, Y., Koresawa, S., Ono, Y., Hayashi, K., 1991. Report on DELP 1988 cruises in the Okinawa Trough, part 3. Crustal structure of the southern Okinawa Trough. Bull. Earthquake Res. Inst 66, 37–70.
Hsu, S.-K., Liu, C.-S., Shyu, C.-T., Liu, S.-Y., Sibuet, J.-C., Serge, L., Wang, C., Donald, R., 1998. New gravity and magnetic anomaly maps in the Taiwan-Luzon region and their preliminary interpretation. Terr. Atmos. Ocean. Sci. 9 (3), 509–532.
Hsu, H.-H., Lin, L.-F., Liu, C.-S., Chang, J.-H., Liao, W.-Z., Chen, T.-T., Chao, K.-H., Lin, S.-L., Hsieh, H.-S., Chen, S.-C., 2019. Pseudo-3D seismic imaging of Geolin Mounds hydrothermal field in the Southern Okinawa Trough offshore NE Taiwan. Terr. Atmos. Ocean. Sci. 30, 705–716. https://doi.org/10.3319/TAO.2019.03.14.02.
Huh, C.-A., Su, C.-C., Wang, C.-H., Lee, S.-Y., Lin, I.-T., 2006. Sedimentation in the Southern Okinawa Trough — rates, turbidites and a sediment budget. Mar. Geol. 231, 129–139.
Inagaki, F., Kuypers, M.M., Tsunogai, U., Ishibashi, J.I., Nakamura, K.I., Treude, T., Hirayama, H., 2006. Microbial community in a sediment-hosted CO_2 lake of the southern Okinawa Trough hydrothermal system. Proc. Natl. Acad. Sci. 103 (38), 14164–14169.
Izawa, E., 1991. Hydrothermal carbonate chimneys in the Iheya Ridge of the Okinawa Trough. JAMSTEC Deep Sea Res. 7, 185–192.
Izawa, Eiji., Motomura, Yoshinobu., Tanaka, Takeo., Kimura, Masaaki., 1991. Hydrothermal carbonate chimneys in the Iheya Ridge of the Okinawa Trough. JAMSTEC Deep Sea Res. 7, 185–192.
Jackson, C.A.-L., Schofield, N., Golenkov, B., 2013. Geometry and controls on the development of igneous sill–related forced folds: a 2-D seismic reflection case study from offshore southern Australia. GSA Bull. 125, 1874–1890.
Johnson, H.P., Becker, K., Von Herzen, R.P., 1993. Near-axis heat flow measurements on the northern Juan de Fuca Ridge: implications for fluid circulation in oceanic crust. Geophys. Res. Lett. 20 (17), 1875–1878. https://doi.org/10.1029/93GL00734.
Johnson, H.P., Tivey, M.A., Bjorklund, T.A., Salmi, M.S., 2010. Hydrothermal circulation within the Endeavour segment, Juan de Fuca Ridge. Geochem. Geophys. Geosyst. 11 (5).
Kao, H., Rau, R.-J., 1999. Detailed structures of the subducted Philippine Sea Plate beneath northeast Taiwan: a new type of double seismic zone. J. Geophys. Res. Solid Earth 104, 1015–1033.
Kimura, M., 1985. Back-arc rifting in the Okinawa Trough. Mar. Pet. Geol. 2, 222–240.
Kimura, M., Uyeda, S., Kato, Y., Tanaka, T., Yamano, M., Gamo, T., Sakai, H., Kato, S., Izawa, E., Oomori, T., 1988. Active hydrothermal mounds in the Okinawa Trough backarc basin, Japan. Tectonophysics 145, 319–324.
Kinoshita, M., Yamano, M., 1997. Hydrothermal regime and constraints on reservoir depth of the Jade site in the Mid-Okinawa Trough inferred from heat flow measurements. J. Geophys. Res. Solid Earth 102, 3183–3194.
Kinoshita, M., Kawada, Y., Tanaka, A., Urabe, T., 2006. Recharge/discharge interface of a secondary hydrothermal circulation in the Suiyo Seamount of the Izu-Bonin arc, identified by submersible-operated heat flow measurements. Earth Planet. Sci. Lett. 245, 498–508.
Lallemand, S., Theunissen, T., Schnürle, P., Lee, C.-S., Liu, C.-S., Font, Y., 2013. Indentation of the Philippine Sea plate by the Eurasia plate in Taiwan: details from recent marine seismological experiments. Tectonophysics 594, 60–79.
Lee, C.S., Shor Jr., G.G., Bibee, L.D., Lu, R.S., Hilde, T.W., 1980. Okinawa Trough: origin of a back-arc basin. Mar. Geol. 35 (1–3), 219–241.
Letouzey, Jean, Kimura, Masaaki, 1986. The Okinawa Trough: genesis of a back-arc basin developing along a continental margin. Tectonophysics 125 (1–3), 209–230.
Li, N., 1988. Study on the fault structure of the Okinawa Trough. Oceanol. Limol. Sin. 19.
Lin, L.F., Hsu, H.H., Liu, C.S., Chao, K.H., Ko, C.C., Chiu, S.D., Hsieh, S.S., Ma, Y.F., Chen, S.C., 2019. Marine 3D seismic volumes from 2D seismic survey with large streamer feathering. Marine Geophys. Res. 40 (4), 619–633.
Lister, C.R.B., 1979. The pulse-probe method of conductivity measurement. Geophys. J. Int. 57, 451–461.
Liu, C.-S., 2018. Geological Investigation of Mineral Resource Potential in the Offshore Northeastern Taiwan: Seismic Reflection and Chirp Sonar investigation (3/4) (No. 107-13-A). Central Geological Survey, Taiwan.
Liu, B., Li, S.-Z., Suo, Y.-H., Li, G.-X., Dai, L.-M., Somerville, I.D., Guo, L.-L., Zhao, S.-J., Yu, S., 2016. The geological nature and geodynamics of the Okinawa Trough, Western Pacific. Geol. J. 51, 416–428.
Lu, R.S., Pan, J.J., Lee, T.C., 1981. Heat flow in the southwestern Okinawa Trough. Earth Planet. Sci. Lett. 55, 299–310.
Luo, C.P., 2001. The Structure of the South Okinawa Trough and the Distribution of Igneous Rocks (Master Thesis). National Taiwan University, Taiwan.
Magee, C., Muirhead, J.D., Karvelas, A., Holford, S.P., Jackson, C.A.L., Bastow, I.D., Schofield, N., Stevenson, C.T.E., McLean, C., McCarthy, W., Shtukert, O., 2016. Lateral magma flow in mafic sill complexes. Geosphere 12, 809–841.
Masaki, Yuka., Kinoshita, Masataka., Inagaki, Fumio., Nakagawa, Satoshi., Takai, Ken., 2011. Possible kilometer-scale hydrothermal circulation within the Iheya-North

field, mid-Okinawa Trough, as inferred from heat flow data. JAMSTEC Rep. Res. Develop. 12, 1–12.
McCaig, A.M., Cliff, R.A., Escartin, J., Fallick, A.E., MacLeod, C.J., 2007. Oceanic detachment faults focus very large volumes of black smoker fluids. Geology 35 (10), 935–938.
Nakamura, M., 2000. Three-dimensional P and S wave velocity structure beneath Japan. Programme Abstracts. In: Seis. Soc. Japan, 2000 Fall Meeting.
Nishizawa, A., Kaneda, K., Oikawa, M., Horiuchi, D., Fujioka, Y., Okada, C., 2019. Seismic structure of rifting in the Okinawa Trough, an active backarc basin of the Ryukyu (Nansei-Shoto) island arc–trench system. Earth Planets Space 71, 21.
Nunoura, T., Takai, K., 2009. Comparison of microbial communities associated with phase-separation-induced hydrothermal fluids at the Yonaguni Knoll IV hydrothermal field, the Southern Okinawa Trough. FEMS Microbiol. Ecol. 67, 351–370.
Planke, S., Rasmussen, T., Rey, S.S., Myklebust, R., 2005. Seismic characteristics and distribution of volcanic intrusions and hydrothermal vent complexes in the Vøring and Møre basins. Geol. Soc. Lond. Petrol. Geol. Conf. Ser. 6, 833–844.
de Ronde Cornel, E.J., Massoth, G.J., Butterfield, D.A., Christenson, B.W., Ishibashi, J., Ditchburn, R.G., Graham, I.J., 2011. Submarine hydrothermal activity and gold-rich mineralization at Brothers Volcano, Kermadec Arc, New Zealand. Mineralium Deposita 46 (5-6), 541–584.
Sakai, H., Gamo, T., Kim, E.S., Tsutsumi, M., Tanaka, T., Ishibashi, J., Oomori, T., 1990. Venting of carbon dioxide-rich fluid and hydrate formation in mid-Okinawa trough backarc basin. Science 248 (4959), 1093–1096.
Scheirer, Daniel S., Shank, Timothy M., Fornari, Daniel J., 2006. Temperature variations at diffuse and focused flow hydrothermal vent sites along the northern East Pacific Rise. Geochem. Geophys. Geosyst. 7, 3.
Sharma, R., Srivastava, P.K., 2014. Hydrothermal fluids of magmatic origin. In: Kumar, S., Singh, R.N. (Eds.), Modelling of Magmatic and Allied Processes, Society of Earth Scientists Series. Springer International Publishing, Cham, pp. 181–208.
Shyu, C.-T., Chang, H.-I., 2005. Determination of seafloor temperatures using data from high-resolution marine He at probes. Terr. Atmos. Ocean. Sci. 16, 137.
Shyu, C.-T., Liu, C.-S., 2001. Heat flow of the southwestern end of the Okinawa trough. Terr. Atmos. Ocean. Sci. 12, 305.
Sibuet, J.-C., Hsu, S.-K., Shyu, C.-T., Liu, C.-S., 1995. Structural and kinematic evolutions of the Okinawa trough backarc basin. In: Taylor, B. (Ed.), Backarc Basins: Tectonics and Magmatism. Springer US, Boston, MA, pp. 343–379.
Sibuet, J.-C., Deffontaines, B., Hsu, S.-K., Thareau, N., Le Formal, J.-P., Liu, C.-S., 1998. Okinawa trough backarc basin: early tectonic and magmatic evolution. J. Geophys. Res. Solid Earth 103, 30245–30267.
Stein, C.A., Stein, S., 2012. Constraints on hydrothermal heat flux through the oceanic lithosphere from global heat flow. J. Geophys. Res. Solid Earth 3081–3095.
Stein, C.A., Von Herzen, R.P., 2001. Geophysical heat flow. In: Steele, J.H. (Ed.), Encyclopedia of Ocean Sciences, Second edition. Academic Press, Oxford, pp. 40–48.
Su, C.-C., 2019. Geological Investigation of Mineral Resource Potential in the Offshore Northeastern Taiwan: Geochemical Investigation and Sea Floor Imaging (4/4) Report of Central Geological Survey, 107-15-A, 220 pp.
Sun, H.-H., 2016. Magmatic-Related Earthquakes in the Southern-Most Okinawa Trough (Master's Thesis). National Taiwan University.
Suzuki, R., Ishibashi, J.-I., Nakaseama, M., Konno, U., Tsunogai, U., Gena, K., Chiba, H., 2008. Diverse range of Mineralization induced by phase separation of hydrothermal fluid: case study of the Yonaguni Knoll IV hydrothermal field in the Okinawa trough back-arc basin. Resour. Geol. 58, 267–288.
Svensen, H., Corfu, F., Polteau, S., Hammer, Ø., Planke, S., 2012. Rapid magma emplacement in the Karoo Large Igneous Province. Earth Planet. Sci. Lett. 325–326, 1–9.
Tsai, C.H., Hsu, S.K., Chen, Y.F., Lin, H.S., Wang, S.Y., Chen, S.C., Cho, Y.Y., 2019. Gas plumes and near-seafloor bottom current speeds of the southernmost Okinawa Trough determined from echo sounders. Terr. Atmos. Ocean. Sci. 30 (5).
Turcotte, D.L., Ahern, J.L., 1977. On the thermal and subsidence history of sedimentary basins. J. Geophys. Res. 1896–1977 (82), 3762–3766.
Watanabe, M., Hoshino, K., Shiokawa, R., Takaoka, Y., Fukumoto, H., Shibata, Y., Shinjo, R., Oomori, T., 2006. Metallic mineralization associated with pillow basalts in the Yaeyama Central Graben, southern Okinawa trough, Japan. In: JAMSTEC Report of Research and Development, 3, pp. 1–8.
Wu, J.-N., Chiang, H.-T., Chiao, L.-Y., Shyu, C.-T., Liu, C.-S., Wang, Y., Chen, S.-C., 2019. Revisiting the data reduction of seafloor heat-flow measurement: the example of mapping hydrothermal venting site around Yonaguni Knoll IV in the South Okinawa Trough. Tectonophysics 767, 228159.
Wu, T.W., Chi, W.C., Lin, Y.S., Chen, S.C., 2019a. Temperature as a tracer for fluid movement at hydrothermal sites near the Yonaguni Knoll IV, Okinawa Trough. Terr. Atmos. Ocean. Sci. 30 (5).
Xiong, Y., Liu, Z., Li, T., Liu, Y., Yu, H., 2018. The sedimentation rates in the Okinawa Trough during the Late Quaternary. Acta Oceanol. Sin. 24 (4), 146–154.
Yamano, M., Uyeda, S., Foucher, J.-P., Sibuet, J.-C., 1989. Heat flow anomaly in the middle Okinawa Trough. Tectonophysics 159, 307–318.
Zhang, X., Zhai, S., Yu, Z., Wang, S., Cai, Z., 2018. Mineralogy and geological significance of hydrothermal deposits from the Okinawa Trough. J. Mar. Syst. 180, 124–131.